Space Science Reviews (2024) 220:64
https://doi.org/10.1007/s11214-024-01096-9

Mass Spectrometer Experiment for a Uranus Probe

Audrey Vorburger[1] · Peter Wurz[1] · Ravit Helled[2] · Olivier Mousis[3,4]

Received: 8 November 2023 / Accepted: 19 July 2024

Abstract
Uranus distinguishes itself from other planets in the Solar System with a range of remarkable attributes, including a magnetosphere with a unique configuration, its quiescent atmosphere, its heating imbalance, its dense and narrow rings, and its unusually dark and tectonically processed icy satellites. Yet no mission to date has investigated either this ice giant or Neptune from up close. A Uranus Orbiter and Probe has thus been identified as the highest-priority new NASA Flagship mission for initiation in the decade 2023–2032. One invaluable instrument on a Uranus probe is a mass spectrometer experiment that analyzes the planet's chemical composition *in situ* in real-time during the probe's descent through the atmosphere. The selection of a mass spectrometer experiment is profoundly driven by the scientific questions the mission seeks to address and necessitates the accurate measurements of crucial elements including their isotope ratios. In addition to fulfilling the posed science requirements, the chosen experiment must adhere to stringent constraints such as mass, power, and size limitations while also prioritizing speed, simplicity of operation, a high level of reliability, and a completely autonomous operation. Here, we offer a succinct overview of the scientific rationale driving the Uranus probe mission, exploring various potential configurations for the mass spectrometer experiment, detailing instruments that complement a mass spectrometer, and discussing key factors that influence the mission's profile. We also address the possibility of a collaborative effort between NASA and ESA, which could play a pivotal role in ensuring the successful development of this groundbreaking mission.

Keywords Uranus · Orbiter and probe · Descent probe · Instrumentation · Atmosphere · Mass spectrometry · Ice giant

1 Introduction

Uranus is one of the least understood planets in the Solar System. The recently completed Decadal Strategy for Planetary Science and Astrobiology 2023–2032 (National Academies

✉ A. Vorburger
audrey.vorburger@unibe.ch

1 Space Research and Planetary Sciences, Physics Institute, University of Bern, Bern, Switzerland

2 Institute for Computational Science, Center for Theoretical Astrophysics & Cosmology, University of Zurich, Zurich, Switzerland

3 Aix-Marseille Université, CNRS, CNES, Institut Origines, LAM, Marseille, France

4 Institut Universitaire de France (IUF), Paris, France

Published online: 22 August 2024

of Sciences, Engineering, and Medicine 2023) selected a Uranus Orbiter and Probe (UOP) as the top priority new Flagship mission for the upcoming decade "primarily for its ability to produce transformative, breakthrough science across a broad range of topics" (ibid p. 618). This paper centers on the scientific insights a probe to Uranus could offer, discussing the crucial role of a mass spectrometer in achieving these scientific objectives. We also outline key factors to consider when planning a mass spectrometer experiment on board such a probe to ensure it can effectively address the anticipated science questions. In short, a Uranus probe can assist in answering two current key questions: (i) When, where, and how did Uranus form and evolve? and (ii) What is the bulk composition of Uranus and its depth dependence? In addition to the science objectives for Uranus, the giant planets in general are natural planetary-scale laboratories for the study of fluid dynamics without the complex effects of topography and ocean-atmosphere coupling. A mass spectrometer experiment aboard a probe can contribute to addressing these scientific questions by offering in situ measurements of chemical composition as a function of depth.

Indeed, mass spectrometers have a long and rich history in the robotic exploration of our Solar System. The first neutral gas mass spectrometers to operate off-ground were two magnetic mass spectrometers that were launched into Earth's atmosphere on an Aerobee rocket in 1963 (Nier et al. 1964). These mass spectrometers measured the Earth's atmospheric composition (detecting mainly N_2 and O) from 104 km up to 209 km. In the following 60 years, mass spectrometers have traveled on a variety of planetary missions, including missions to Mercury (BepiColombo), Venus (Pioneer Venus Multiprobe and Orbiter, Vega 1 and 2, and Venera 4–14), the Moon (Apollo 15–17, Chandrayaan-1 and -2, LADEE, and Luna Resurs), Mars (Viking 1 and 2, Phoenix, Mars Science Laboratory, Mars Orbiter Mission, and MAVEN), Jupiter (Galileo), Saturn's moon Titan (Cassini-Huygens), and to comets 1P/Halley (Giotto) and 67P/Churyumov-Gerasimenko (Rosetta). Collectively, these missions have significantly advanced our understanding of the celestial bodies that encompass our Solar System. They have provided us with invaluable data regarding the distribution of a diverse array of elements and molecules across our Solar System, encompassing atomic hydrogen (H), molecular hydrogen (H_2), deuterium (HD), helium isotopes (^{3}He and ^{4}He), noble gases (Ne, Ar, Kr, Xe), as well as essential compounds like oxygen (O and O_2), nitrogen (N_2), carbon monoxide (CO), carbon dioxide (CO_2), methane (CH_4), ammonia (NH_3), water (H_2O), hydrogen sulfide (H_2S), hydrogen chloride (HCl), and a variety of hydrocarbons. Notably, the list of species measured by the mass spectrometers on board Rosetta alone contains more than 100 species (Le Roy et al. 2015; Rubin et al. 2019a). This wealth of information has not only expanded our knowledge of our Solar System but has also deepened our insights into the atmospheric compositions of planetary bodies, informing us about the formation, evolution, and dynamics of our celestial neighborhood, atmospheric processes (e.g., climate and weather patterns), planetary interiors, and the origin of volatiles, including water.

Even with the James Webb Space Telescope being in operation and planned future extremely large Earth-based telescopes (GMT, TMT, E-ELT), mass spectrometers will remain key instruments in the *in situ* exploration of the ice giants Uranus and Neptune, which represent a largely unexplored class of planetary objects filling the gap in size between the larger gas giants and the smaller terrestrial worlds. Our knowledge of Uranus is sparse since so far the planet has never had a dedicated mission, but only a single short flyby by Voyager-2 in the 1980s, and the information that can be inferred from ground-based observation is limited. Currently, there are thus many key open questions linked to the origin, evolution, and internal structure of Uranus (see, e.g., Fletcher et al. 2022; Helled et al. 2020; Mousis et al. 2022; Helled and Fortney 2020; Guillot et al. 2020). Constraining the internal structure and

atmospheric composition of Uranus can reveal fundamental information on its formation and evolutionary path, and more generally on the origin of the solar system. The Galileo probe measurements made at Jupiter perfectly represent the key measurements that cannot be achieved via remote sensing. For instance, they have shown the unexpected enrichments of Ar, Kr, and Xe with respect to their solar abundances (see Fig. 2), which suggests that the icy building blocks accreted by the planet formed at temperatures possibly below ∼50 K to enable the trapping of these noble gases (Owen et al. 1999; Gautier et al. 2001; Mousis et al. 2009). Another key measurement is the determination of the helium abundance, which was accomplished at Jupiter by using a dedicated Jamin interferometer that measured precisely the refractive index of the atmosphere aboard the Galileo probe with an accuracy of 2% (von Zahn et al. 1998). Such an accuracy on the He/H_2 ratio is impossible to derive remotely in giant planet atmospheres and yet precise knowledge of this ratio is crucial for understanding their internal structures and thermal evolution. The Voyager mission has already shown that these ratios are far from being identical in the gas and ice giants, which would presumably result from different thermal histories and internal processes at work (Helled et al. 2020). As discussed in this paper, today's mass spectrometers have the capability to measure the helium abundance at the same level of accuracy. Another significant finding from the mass spectrometer on the Galileo probe was its determination of Jupiter's $^{15}N/^{14}N$ ratio, measured at $(2.3 \pm 0.3) \times 10^{-3}$. This result indicates that the nitrogen currently found on Jupiter likely originated from the solar nebula predominantly in the form of N_2 (Owen et al. 2001). Remote-sensing observations, if possible, do not have the same accuracy, as illustrated by the upper limit set on the $^{15}N/^{14}N$ ratio at Saturn ($\leq 2.8 \times 10^{-3}$) by NASA's Infrared Telescope Facility (Fletcher et al. 2014).

Furthermore, despite the otherwise outstanding performances of the novel ground- and space-based telescopes, remote sensing of giant planet atmospheres provides access to only a limited range of altitudes depending on the used wavelength, summarized in Fig. 1. Ultraviolet (UV) radiation is used to explore the upper atmosphere down to approximately 10^{-1} mbar in the thermosphere (Atreya et al. 2019). This range allows scientists to gather data primarily on the various hydrocarbons produced by ongoing photochemical processes in the thermosphere (Moses et al. 2018). Infrared (IR) radiation is used to study the photochemical layer, with a probing depth that ranges from approximately 10–1000 mbar, depending on the specific species being observed. This method provides insights into the hydrocarbons formed within this layer due to photochemistry. It also allows researchers to detect and analyze other compounds such as carbon monoxide, hydrogen cyanide, and additional trace gases present within this atmospheric zone. Visible radiation can be used to gather information down to the tropospheric hazes and the uppermost layer of methane (CH_4) clouds, which are expected to be located within the pressure range of 0.2–1 bar (Hueso and Sánchez-Lavega 2019). This range allows researchers to study atmospheric structures and weather patterns, offering insights into cloud formation and dynamics at these deeper atmospheric levels. Microwave opacity in an atmosphere is influenced by its chemical composition, allowing microwave brightness measurements across a range of frequencies to be inverted to derive the abundances of specific gases like ammonia (NH_3), water (H_2O), and potentially hydrogen sulfide (H_2S). This method can be used to probe atmospheric depths at or below the cloud deck. The Juno mission, for example, employed this approach to study Jupiter's atmosphere (Bolton et al. 2017). The vertical resolution of "nadir" remote sensing is limited to the width of the contribution function, i.e., the range of altitudes contributing to the upwelling radiance at a given wavelength, which can extend over one or more scale heights and makes it impossible to uniquely identify the temperature and density perturbations associated with cloud formation, wave phenomena, etc. *In situ* exploration of Uranus' atmosphere by a descending atmospheric probe would provide direct sampling and "ground-truth" for the myriad of

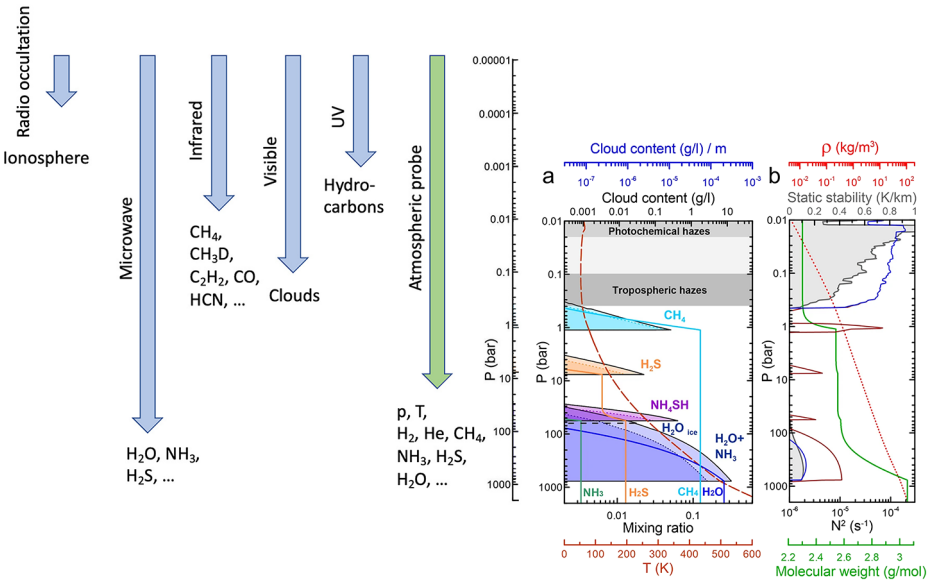

Fig. 1 Information depth of various remote sensing spectroscopic techniques (blue), the microwave measurements limited by the opacity of the atmosphere (Bolton et al. 2017), and the measurements of an atmospheric probe assumed to operate down to the 20 bar level (green), in comparison with a model of Uranus' atmosphere and clouds from Hueso and Sánchez-Lavega (2019). Reproduced with permission from Hueso and Sánchez-Lavega (2019), copyright by Springer

physical and chemical processes at work in their atmospheres with good vertical resolution. A probe will provide direct measurements of pressure, temperature, and other physical parameters, and it will provide detailed chemical composition from mass spectrometry with fine altitude resolution.

This paper aims to detail the primary considerations for implementing a mass spectrometer experiment on a probe to Uranus and to propose a European-led probe that could potentially be integrated into the UOP mission to Uranus. A UOP would contribute to several priority science question topics as identified in the Decadal Survey (National Academies of Sciences, Engineering, and Medicine 2023), in particular to Q7 (Giant planet structure and evolution), Q8 (Circumplanetary systems), and Q12 (Exoplanets), but also to Q2 (Accretion in the outer solar system), Q1 (Evolution of the protoplanetary disk), Q4 (Impacts and dynamics), and Q5 (Solid body interiors and surfaces), and, modestly, to Q10 (Dynamic Habitability). Moreover, incorporating a mass spectrometer aboard the probe presents a unique opportunity to delve into two crucial aspects. Firstly, it enables a comprehensive exploration of atmospheric circulation within an ice giant, elucidating the dynamics from the interior to the thermosphere. This entails resolving the composition and mapping of disequilibrium species such as CH_4, H_2S, H_3^+, C_2H_2, and C_2H_6 at depths of less than 3 bars. Secondly, it facilitates an in-depth investigation into the formation and evolutionary journey of Uranus, shedding light on its thermal and spatial evolution, including any migration phenomena. This involves constraining noble gas abundances, encompassing isotopes of helium and xenon, as well as elemental and isotope abundances of hydrogen, carbon, sulfur, nitrogen, and oxygen.

This paper is structured as follows: In Sect. 2, we present the scientific rationale behind sending a probe to Uranus, which in turn informs the essential design driver for the mass spectrometer experiment. Section 3 provides a comprehensive discussion of mass spectrom-

eter systems in their entirety. This includes an examination of various options for the ionization source, the mass analyzer, and the detector, all critical components of the experiment. In Sect. 4, we highlight the potential for synergy between a mass spectrometer and other instruments that could be part of a Uranus probe. These collaborative measurements can significantly enhance our scientific understanding of the planet's atmosphere, environment, and interior. Finally, in Sect. 5, we present a detailed proposal for the implementation of a mass spectrometer experiment tailored to the unique requirements of a Uranus probe mission. This proposal encompasses considerations related to probe entry and the potential complementarity with an atmospheric orbiter, offering a comprehensive vision for the mission's scientific objectives.

2 Science Motivation

Tables 1 and 2 provide a comprehensive overview of our current knowledge of the elemental abundances and isotope ratios within the atmospheres of Jupiter, Saturn, Uranus, and Neptune. Jupiter, thanks to the dedicated Galileo mission, stands as a shining example of the wealth and accuracy of information we can obtain when a probe is dispatched into the atmosphere of a giant planet. In contrast, Saturn, Uranus, and Neptune, which have yet to receive dedicated probes, suffer from a significant paucity of information. The lone exception lies in the C/H ratio of Saturn, which we have gleaned from Cassini's observations. Tables 1 and 2 thus strikingly underscore the vast disparity between the knowledge gained from *in situ* sampling during a planetary mission (i.e., Galileo probe at Jupiter) and that possibly gained through remote observations from planetary missions (e.g., Cassini and Voyager) and space-based telescopes (e.g., ISO, HST, and JWST) as well as Earth-based observatories (e.g., IRTF and Gemini). Simultaneously, the tables poignantly expose our profound gaps in understanding the compositions of the unprobed giant planets.

Measuring the elemental abundances in Uranus' atmosphere by a probe not only provides a boundary condition to interior models but can also discriminate among different formation scenarios for Uranus. Planet formation models still struggle to explain the final mass and composition of Uranus. Standard formation models cannot easily lead to the formation of an intermediate-mass planet with a hydrogen-helium (H-He) mass fraction of $\sim$10%. Often the planets in this mass range have smaller H-He atmospheres, or, alternatively, they become gas giant planets. Fine-tuning the formation models is required to get a planet that is similar to Uranus in terms of its physical properties (e.g., Helled and Bodenheimer 2014; Valletta and Helled 2022). Various solutions have been proposed that could overcome this challenge, including formation at closer radial distances followed by outward migration, formation via pebble accretion, and slow formation where the onset of gas accretion occurs during or after the gas disk dissipation (see Helled et al. 2020 for further discussion). At the moment, no theory provides a satisfactory solution for Uranus' formation, and each solution has some disadvantages.

A fundamental measurement is that of the helium abundance, which needs to be refined at the level of the one performed in Jupiter's atmosphere by the Galileo probe (see Table 1) and compared to the protosolar value. Helium rain is unlikely to occur in Uranus (unlike in the case of Saturn, and, probably, Jupiter) although this is still being investigated (Stevenson and Salpeter 1977; Fortney and Hubbard 2004; Bailey and Stevenson 2021). If indeed helium rain does not occur in Uranus, then a measurement of the helium abundance in the atmosphere should be representative of the bulk composition, and therefore this measurement can constrain the formation timescale of Uranus. One explanation of why Uranus did

not reach runaway gas accretion, and therefore did not become a gas giant planet, is that it formed slowly, on a timescale comparable to the disk's lifetime, and by the time Uranus started to accrete gas from the disk more efficiently, the disk began to dissipate (Helled and Bodenheimer 2014; Valletta and Helled 2022; Helled 2023; Eriksson et al. 2023). In that case, Uranus would be enriched with noble gases, and possibly, have a higher helium-to-hydrogen ratio compared to the protosolar composition.

Another crucial measurement is the determination of the abundances of heavy noble gases. Currently, it is unknown whether most of Uranus' building blocks came from an outer reservoir of pristine ices preserved from the protosolar molecular cloud, an inner reservoir of crystalline ice, or an intermediate reservoir that was only moderately heated to a point where all volatiles except water were vaporized. Measuring the noble gas abundances in Uranus' atmosphere can thus help constrain the composition of Uranus' building blocks (Mandt et al. 2020). Additionally, by measuring the noble gas content in Uranus' atmosphere and comparing it to the measurements made by the Galileo spacecraft in Jupiter's atmosphere (as shown in Table 1), we can conduct the first "comparative planetology" in the outer Solar System. This comparison can help determine whether the atmospheric compositions of the two planets were influenced by the same enrichment processes and if this enrichment in noble gases could be attributed to late-stage gas accretion (Guillot and Hueso 2006; Mousis et al. 2020; Helled 2023).

A further key result would be the precise determination of the D/H ratio in Uranus, complemented by the measurement of the $^{3}He/^{4}He$ ratio in its atmosphere, to provide further constraints on the protosolar D/H ratio, which remains relatively uncertain (see Table 2). Deuterium enrichment, observed by the Herschel space-based telescope in both Uranus and Neptune, appears to be remarkably similar between the two planets. This elevated deuterium-to-hydrogen ratio suggests that considerable mixing occurred between the protosolar H_2 and the H_2O ice that the planets accreted (Feuchtgruber et al. 2013).

Moreover, the $^{14}N/^{15}N$ ratio presents large variations in the different planetary bodies in which it has been measured (see Table 2 for instance), and consequently, remains difficult to interpret. A 1–σ lower limit for the $^{14}N/^{15}N$ ratio has been found to be $\sim$500 in Saturn's ammonia from TEXES/Infrared Telescope Facility ground-based mid-infrared spectroscopic observations (Fletcher et al. 2014). This lower limit is formally consistent with the $^{14}N/^{15}N$ ratio ($\sim$435) measured by the Galileo probe at Jupiter (Owen et al. 2001) and implies that the two giant planets were essentially formed from the same nitrogen reservoir in the nebula, which is N_2 (Owen et al. 2001; Fletcher et al. 2014; Mousis et al. 2014). Measuring $^{14}N/^{15}N$ in the atmospheres of Uranus and Neptune would provide important insights into the origin of the primordial nitrogen reservoir in these planets.

The isotopic measurements of carbon, oxygen, and noble gases should ideally reflect their primordial values. For instance, minimal variations are typically observed in the $^{12}C/^{13}C$ ratio across different celestial bodies and molecules within the Solar System. As indicated in Table 2, the ratios measured in the atmospheres of Jupiter and Saturn align closely with the terrestrial value of 89 (Niemann et al. 1998; Fletcher et al. 2009a). A novel in situ assessment of this ratio in Uranus and/or Neptune would be invaluable in corroborating whether their carbon isotopic ratio also mirrors that of Earth. The Galileo probe's measurements in Jupiter's atmosphere revealed that the heavy noble gas isotope ratios are protosolar. Measuring the heavy noble gas isotope ratio in Uranus' atmosphere would help determine if the heavy noble gases in the ice giant's atmosphere share a common nucleosynthetic source, similar to the xenon in comet 67P/Churyumov-Gerasimenko, as inferred from Rosetta's isotope measurements (Marty et al. 2017).

We refer the reader to the review of Mousis et al. (2022) for further discussion about the key isotope and element abundances to be measured in Uranus.

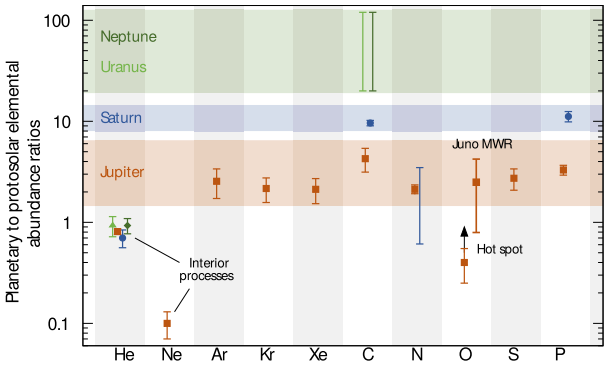

Fig. 2 Enrichment factors (with respect to the protosolar value) of noble gases and heavy elements measured in Jupiter, Saturn, Uranus, and Neptune. Error bars, central values, and planets share the same color codes. Both oxygen determinations from Galileo (hot spot) and Juno (Juno MWR) at Jupiter are shown in the diagram. All data values are taken from Mousis et al. (2018), except the Juno value, which is taken from Cavalié et al. (2023)

Our understanding of the ice giants in our solar system, Uranus and Neptune, is notably limited. A future mission to Uranus, equipped with a mass spectrometer, must aim to address this knowledge gap. The mission should seek to capture the same level of detail and accuracy in its data as we've achieved with Jupiter, helping to close the gaps in our understanding of elemental abundances for these planets.

At the same time, it should be kept in mind that there are caveats associated with the measurements and their link to planet formation due to the complex and somewhat degenerate nature of the problem. Distinguishing between formation processes in the outer disk and the accretion of building blocks from outer regions is challenging, complicating the determination of whether a planet formed slowly or simply late. Additionally, a probe's measurements are limited to the outermost layer of the atmosphere, which might not fully represent the planet's bulk composition. Despite these caveats, obtaining detailed atmospheric composition data from Uranus is crucial for advancing our understanding of the planet's characteristics and will provide valuable insights into its interior structure, evolutionary history, and origin.

3 Mass Spectrometer Experiment

Mass spectrometers allow direct identification and quantification of atoms and molecules present in a given sample of the atmosphere. As such, they operate *in situ*, providing ground truth about the local environment without the necessity of complicated inference as, for example, remote sensing requires. Moreover, when interpreting mass spectrometric measurements, degeneracy poses a significantly lesser concern compared to its impact on spectroscopic measurements. On the downside, mass spectrometers can only analyze their immediate vicinity, requiring them to be placed within the environment of interest. An *in situ* atmospheric probe for Uranus would thus offer an ideal platform for conducting mass spectrometry and precisely analyzing the composition of Uranus' atmosphere.

A mass spectrometer experiment designed to analyze the atmosphere of a giant planet during a probe's descent consists of four key components: a sample introduction system, an ionization source, the mass analyzer itself, and the detector. In the following, we will discuss each component separately, before we make a suggestion for a mass spectrometer experiment suitable to a Uranus probe in Sect. 5.

Table 1 Elemental abundances in Jupiter, Saturn, Uranus, and Neptune, as derived from upper tropospheric composition measurements

Elements	Jupiter	Saturn	Uranus	Neptune
He/H[(1)]	$(7.85 \pm 0.16) \times 10^{-2}$	$(6.75 \pm 1.25) \times 10^{-2}$	$(8.88 \pm 2.00) \times 10^{-2}$	$(8.96 \pm 1.46) \times 10^{-2}$
Ne/H[(2)]	$(1.240 \pm 0.014) \times 10^{-5}$	–	–	–
Ar/H[(3)]	$(9.10 \pm 1.80) \times 10^{-6}$	–	–	–
Kr/H[(4)]	$(4.65 \pm 0.85) \times 10^{-9}$	–	–	–
Xe/H[(5)]	$(4.45 \pm 0.85) \times 10^{-10}$	–	–	–
C/H[(6)]	$(1.19 \pm 0.29) \times 10^{-3}$	$(2.65 \pm 0.10) \times 10^{-3}$	$(0.6 - 3.2) \times 10^{-2}$	$(0.6 - 3.2) \times 10^{-2}$
N/H[(7)]	$(3.32 \pm 1.27) \times 10^{-4}$	$(0.50 - 2.85) \times 10^{-4}$	–	–
O/H[(8)]	$(2.45 \pm 0.80) \times 10^{-4}$	–	–	–
O/H[(9)]	$(1.45^{+1.27}_{-0.93}) \times 10^{-3}$	–	–	–
S/H[(10)]	$(4.45 \pm 1.05) \times 10^{-5}$	–	$(5 - 12.5) \times 10^{-6}$	$(2.0 - 6.5) \times 10^{-6}$
P/H[(11)]	$(1.08 \pm 0.06) \times 10^{-6}$	$(3.64 \pm 0.24) \times 10^{-6}$	–	–

[(1)] von Zahn et al. (1998), Niemann et al. (1998) for Jupiter, Conrath and Gautier (2000) for Saturn, Conrath et al. (1987) for Uranus and Burgdorf et al. (2003) for Neptune. We only consider the higher value of the uncertainty on He in the case of Neptune. [(2–5)] Mahaffy et al. (2000) for Jupiter. [(6)] Wong et al. (2004) for Jupiter, Fletcher et al. (2009a) for Saturn, Lindal et al. (1987), Baines et al. (1995), Karkoschka and Tomasko (2009), Sromovsky et al. (2014) for Uranus, Lindal et al. (1990), Baines et al. (1995), Karkoschka and Tomasko (2011) for Neptune. [(7)] Wong et al. (2004) for Jupiter, Fletcher et al. (2011) for Saturn (N/H range derived from the observed range of 90–500 ppm of NH_3). [(8)] Wong et al. (2004) for Jupiter (Galileo probe determination, probably a lower limit, not representative of the bulk O/H). [(9)] Li et al. (2020) for Jupiter (Juno determination). [(10)] Wong et al. (2004) for Jupiter, lower limits for Uranus Irwin et al. (2018) and Neptune Irwin et al. (2019). [(11)] Fletcher et al. (2009b) for Jupiter and Saturn.

3.1 Sample Introduction System

The operating conditions for a mass spectrometer, including its sample inlet choice, are contingent on the ambient pressure. When the ambient pressure remains below approximately $\sim 10^{-6}$ mbar, the instrument can employ a direct gas inlet. However, if the ambient pressure exceeds this threshold, typically at or above 10^{-6} mbar, integration of the mass spectrometer into a vacuum system becomes necessary. This integration, in turn, mandates the implementation of a sophisticated sample inlet subsystem. A suitable sample inlet subsystem for a mass spectrometer experiment on board a Uranus probe is proposed in Sect. 5.

3.2 Ionization Source

Since all mass spectrometers use some kind of electromagnetic field to separate ions of different masses, ionization of the neutral gas is necessary. Various techniques can be employed for ionization, with the most common methods used for gaseous samples being electron-impact ionization, photo-ionization, chemical ionization, and field ionization. For further information on ionization sources, please see Ashcroft (2007).

Electron Ionization: In electron ionization (also referred to as electron-impact ionization), low-energy electrons are directed toward the neutral gas. These incoming electrons typically carry energies ranging from 70 to 100 eV, well surpassing the ionization potential of most atoms and molecules, which falls below 25 eV, and often is around 10 eV. In this process, the incoming electron dislodges one or more electrons from the neutral atom or molecule,

Table 2 Isotope ratios measured in Jupiter, Saturn, Uranus, and Neptune

isotope ratio	Jupiter	Saturn	Uranus	Neptune
D/H (in H_2)[(1)]	$(2.60 \pm 0.7) \times 10^{-5}$	$1.70^{+0.75}_{-0.45} \times 10^{-5}$	$(4.4 \pm 0.4) \times 10^{-5}$	$(4.1 \pm 0.4) \times 10^{-5}$
^{3}He/^{4}He[(2)]	$(1.66 \pm 0.05) \times 10^{-4}$	–	–	–
^{12}C/^{13}C (in CH_4)[(3)]	$92.6^{+4.5}_{-4.1}$	$91.8^{+8.4}_{-7.8}$	–	–
^{14}N/^{15}N (in NH_3)[(4)]	434.8^{+65}_{-50}	> 357	–	–
^{20}Ne/^{22}Ne[(5)]	13 ± 2	–	–	–
^{36}Ar/^{38}Ar[(6)]	5.6 ± 0.25	–	–	–
^{136}Xe/total Xe[(7)]	0.076 ± 0.126	–	–	–
^{134}Xe/total Xe[(8)]	0.091 ± 0.074	–	–	–
^{132}Xe/total Xe[(9)]	0.290 ± 0.068	–	–	–
^{131}Xe/total Xe[(10)]	0.203 ± 0.088	–	–	–
^{130}Xe/total Xe[(11)]	0.038 ± 0.138	–	–	–
^{129}Xe/total Xe[(12)]	0.285 ± 0.075	–	–	–
^{128}Xe/total Xe[(13)]	0.018 ± 0.094	–	–	–

[(1)] Mahaffy et al. (1998) for Jupiter, Lellouch et al. (2001) for Saturn, Feuchtgruber et al. (2013) for Uranus and Neptune.

[(2)] Mahaffy et al. (1998) for Jupiter.

[(3)] Niemann et al. (1998) for Jupiter, Fletcher et al. (2009b) for Saturn.

[(4)] Wong et al. (2004) for Jupiter, Fletcher et al. (2014) for Saturn.

[(5−13)] Mahaffy et al. (2000) for Jupiter.

resulting in its conversion into a positive ion. Electron impact ionization is renowned for its high efficiency and simplicity; however, it is classified as a "hard ionization" technique because in addition to ionizing the parent molecule it also causes significant fragmentation of the molecule, thus adding fragment ions to the mass spectra. This occurs because the electron energy used is much higher than the ionization potential of the atoms and molecules. As a result, some of this excess energy is transferred to the molecules, leading to the break-up of many parent molecules into fragment ions. Even though fragmentation is usually undesired, the fragments may offer information on the chemical structure of molecules, for example on isomers. Interpreting electron ionization mass spectra, including the fragment ions, is a very established technique in mass spectrometry (e.g. McLafferty and Turecek 1993).

Photo-Ionization: In contrast to electron impact ionization, photo-ionization employs a photon beam to achieve ionization. For this process to occur successfully, the photons used must possess energy equal to or larger than the ionization potential, leading to the common use of UV photons for atoms and molecules with ionization potentials exceeding ∼5 eV. It's worth noting that photo-ionization cross-sections tend to be typically 10–100 times smaller than their electron-impact ionization counterparts, which makes this method less efficient. To compensate for this, more intense photon sources are required, typically laser sources. On the plus side, this ionization technique falls under the category of "soft ionization" since it keeps the parent molecules mostly intact and generates only few fragment ions during the process.

Chemical Ionization: Chemical ionization is a technique where neutral gas is ionized through ion-molecule reactions in the presence of a large excess of an ionizing gas providing

reactants (Harrison 2017). Frequently used gases for chemical ionization include methane, isobutane, and ammonia, all of which generate positive ions. This method is known for producing minimal ion fragmentation, making it particularly valuable for ionizing larger molecules. Consequently, it falls under the category of "soft ionization." However, chemical ionization comes with larger experimental complexity, as a supply of the ionizing gas needs to be provided and the reactants have to be formed in the ionizing gas. Moreover, the typical reactant gases are the same as some of the species to be investigated in Uranus' atmosphere, thus rendering this ionization method less suitable to this case.

Field Ionization: Field ionization mass spectrometry can detect molecules that are volatile in vacuum, or which form during pyrolysis in vacuum. The method works by passing molecules in the gas phase through a strong electric field between a sharp point or edge and an earthed electrode (Beckey 1970). Field ionization is notable for its capacity to not only minimize the production of fragment ions and but also to reduce the generation of excited ions compared to other ionization techniques. However, excited molecular ions can fragment later as they move through the mass analyzer, resulting in signals appearing in random locations within the mass spectrum. This unwanted noise is referred to as chemical noise in mass spectrometry. To achieve the necessary high electric field strength for field ionization, filaments with numerous micrometer-sized whiskers are employed. However, this method presents some unique experimental challenges. Given the substantial geometrical extent of the array of whiskers, the high field strengths, and the small ion yield for a given sample, this ionization technique requires specialized ion-optical elements for effective ion collection and focusing into the mass analyzer.

3.3 Mass Analyzer

For the mass analyzer itself, a range of types is available, each tailored for specific applications. The most widely used types are magnetic sector mass analyzers, quadrupole mass analyzers, time-of-flight mass analyzers, ion trap mass analyzers, and Orbitrap mass analyzers. It's important to note that among these five, only the first four have been used in space missions, demonstrating flight heritage. An additional noteworthy aspect regarding the flight adaptability of these mass spectrometers is that many of the models used in space missions have primarily focused on measuring thin atmospheres. While the mass analyzers themselves remain relevant for a Uranus probe, the higher density of its atmosphere poses additional challenges, necessitating supplementary systems such as a vacuum system, an adapted gas inlet, and a tailored mission profile.

In the following paragraphs, we will provide a concise overview of each mass analyzer type, enumerate the missions that have incorporated them (excluding Earth missions), and outline the distinct advantages and limitations associated with each type in view of an application on an atmospheric probe. Table 3 provides an assessment of the different types of mass analyzers discussed herein, with a focus on their suitability for a Uranus probe. This evaluation outlines the pros and cons of each type, helping to determine which mass analyzer is most appropriate for the unique conditions encountered during a mission to Uranus. References for the different mass spectrometer types are given at the end of each paragraph. Readers are encouraged to also consult Arevalo et al. (2020) and Chou et al. (2021), two comprehensive papers that delve into the intricacies of mass spectrometry in space exploration, including thorough discussions on past flown mass spectrometers.

Table 3 Evaluation of pros and cons of the major mass spectrometer types in view of an application on the Uranus atmospheric probe

	Pros	Cons
Magnetic Sector	- high mass resolution possible ($m/\Delta m \sim 9{,}000$)	- large size and mass
	- sufficient mass range for atmospheric probe	- need for magnet
	- high accuracy isotope measurements	- mechanically complex
	- electronics comparatively simple	- either high transmission or mass resolution
	- ample flight heritage	- scanning instrument (complete mass spectra at low cadence)
Quadrupole	- unit mass resolution ($m/\Delta m \sim 100$–150)	- either high sensitivity or mass resolution
	- sufficient mass range for atmospheric probe	- sensitivity depends highly on electronic settings
	- good sensitivity for certain applications	- sensitivity is mass-dependent
	- simple, robust method	- susceptible to pollution of the ion optics
	- compatible with many ion sources	- scanning instrument (complete mass spectra at low cadence)
	- ample flight heritage	
Time-of-flight	- high mass resolution ($m/\Delta m \sim 5,000$–$50,000$)	- complicated electronics
	- large mass range (limited only by size of memory)	- very high data rate
	- high dynamic range and sensitivity	- need for onboard data processing
	- capable of measuring isotope ratios	
	- no mass scanning (complete mass spectra at high cadence)	
	- compatible with many ion sources	
	- ample flight heritage	
Ion trap	- medium mass resolution ($m/\Delta m \sim 100$–$1,000$)	- external ion source complicated (requires ion trap insertion)
	- ion manipulation and ion selection possible	- space charge limits dynamic range and isotope measurements
	- storage of ions possible	- sensitivity depends on settings
	- coupling to other mass spectrometers possible	- sensitivity is mass-dependent
	- flight heritage	- susceptible to pollution of the ion optics
		- scanning instrument (complete mass spectra at low cadence)

Magnetic Sector Mass Spectrometers: Magnetic sector field mass spectrometers rely on magnetic fields, sometimes in combination with electric fields, to segregate and analyze ions (Benninghoven et al. 1987). Within the instrument, charged particles experience a force exerted by these fields, guiding them along curved trajectories determined by their mass-to-charge ratio (m/z). The instrument's geometry and precisely calibrated magnetic field strength ensure that only ions with specific m/z ratios reach the detector. Fine-tuning

Table 3 (*Continued*)

	Pros	Cons
Orbitrap	- very high mass resolution (m/Δ m ~500,000)	- needs very highly stable high voltage
	- very small volume of mass analyser	- small ion-optical phase space
	- low sampling frequency	- requires complicated ion optics for ion transfer
	- low mass of mass analyser	- needs phased operation (ion production, insertion, measurement, and instrument cleaning)
	- low power demands	- requires a high level of mass calibration when high mass accuracy is needed
	- positive and negative ions measurable	- dynamic range limited by space charge and Fourier transform principle
	- all ions analyzed simultaneously	- difficult to obtain isotope ratios
	- no detector, thus no detector degradation	- no flight heritage

the magnetic field strengths, or the ion energy, permits the selective detection of ions with varying mass-to-charge ratios. In essence, only ions with the correct momentum reach the detector while ions with incorrect momentum are effectively prevented from doing so. Furthermore, by adding an electrostatic sector in the ion-optical system, ions can undergo further sorting based on their kinetic energy. This enables only ions with a specific energy level to pass through the instrument, adding another layer of selectivity and control to the analysis.

Magnetic sector mass spectrometers provide adequate coverage of the required mass range for a Uranus probe, offering high mass resolution and, consequently, high accuracy for isotope measurements. The electronics operating such systems are relatively straightforward when compared to other mass spectrometer types, and magnetic field mass spectrometers have a well-established history of successful deployment in space missions. Limitations of this mass spectrometer type are that they come with substantial size and mass requirements, and necessitate the incorporation of magnets, which introduce their own set of challenges. Moreover, magnetic sector mass spectrometers cannot optimize for both ion transmission and resolution at the same time. Finally, to obtain a comprehensive mass spectrum, a mass scan is required, which is a time-consuming process for these instruments. This characteristic makes magnetic sector mass spectrometers less suitable for a Uranus probe mission, where speed and efficiency are crucial due to the constraints of the mission profile.

Magnetic sector MS have flown on Apollo 15 through 17 (LACE Hoffman et al. 1972, 1973) to the Moon, on Phoenix (TEGA Hoffman et al. 2008) and on Viking 1 & 2 (GCMS Nier and McElroy 1977; Rushneck et al. 1978) to Mars, on the Pioneer missions (BNMS, LNMS Taylor et al. 1980) to Venus, on Giotto (NMS Krankowsky et al. 1986; Balsiger et al. 1987) to comet 1P/Halley, and on Rosetta (ROSINA Balsiger et al. 1998, 2007; Glassmeier et al. 2007; Wurz et al. 2015; Rubin et al. 2019b) to comet 67P/Churyumov–Gerasimenko.

Quadrupole Mass Spectrometers: Quadrupole mass spectrometers employ a combination of static and dynamic electric fields, created by four cylindrical or hyperbolic rod electrodes arranged in parallel at equidistant positions from a central axis (Dawson 1979). This configuration serves to separate and analyze ions based on their mass-to-charge ratio (m/z). Within

the quadrupole, ions undergo periodic oscillations in response to the electric fields generated by the rods. These oscillations permit only ions with specific m/z ratios, matching the analyzer's predefined settings, to follow stable trajectories as they traverse the rod system and eventually reach the detector. Ions possessing different m/z values experience unstable trajectories, leading to collisions with the rod system. To cover a range of mass values, similar to magnetic sector field mass spectrometers, it is essential to perform a mass scan. This is achieved by adjusting the voltages applied to the quadrupole rods, enabling the instrument to selectively analyze ions across the desired mass range.

Quadrupole mass spectrometers offer a straightforward and reliable approach for *in situ* analysis of Uranus' atmosphere. They encompass an adequate mass range and deliver the required mass resolution for the mission's objectives. Additionally, quadrupole mass spectrometers exhibit commendable sensitivity to Uranus' atmospheric gases, offer compatibility with various ion sources, and have a robust track record in previous space missions. Drawbacks of quadrupole mass spectrometers include the fact that they can optimize either sensitivity or mass resolution, but not both simultaneously. Moreover, their sensitivity is subject to electronic settings and mass-dependent variations, and they are vulnerable to contamination of the ion optics. Finally, akin to magnetic sector mass spectrometers, quadrupole mass spectrometers operate as scanning instruments, which do not align optimally with the mission profile of a descending probe characterized by a one-time, time-constrained mission.

Quadrupole mass spectrometers have a long history in planetary research. They have been included in the Pioneer missions (ONMS Colin 1979; Niemann et al. 1980; Taylor et al. 1980) and on the Venera 5 to Venera 14 missions (OVSP, VNMS Istomin et al. 1980; Istomin 1982) to Venus, on Galileo (GPMS Niemann et al. 1992) to Jupiter, on Cassini-Huygens (GCMS, INMS Niemann et al. 2002, 2005, 2010; Waite et al. 2004) to Titan, on Chandrayaan-1 (CHACE Sridharan et al. 2010) and LADEE (NMS Mahaffy et al. 2014) to Earth's Moon, and on Mars Orbiter Mission (MENCA Bhardwaj et al. 2016), Mars Science Laboratory (SAM/QMS Mahaffy et al. 2012), and MAVEN (NGMS Mahaffy et al. 2015) to Mars.

Time-of-Flight Mass Spectrometers: Time-of-flight mass spectrometers operate by precisely measuring the flight time of ions, all accelerated to the same kinetic energy, as they traverse a defined distance (Cotter 1997). Initially, these ions are accumulated within an ion storage region before being propelled into a drift region by an extraction pulse (Abplanalp et al. 2010). Inside the drift region, ions undergo separation based on their mass-to-charge ratio (m/z). This separation process results in lighter ions reaching the detector ahead of their heavier counterparts, where each ion's time of flight directly corresponds to the square root of its m/z value. By meticulously recording the arrival times of ion packets at the detector, the instrument generates a mass spectrum. This capability allows for the simultaneous and comprehensive analysis of all species without the necessity of individually scanning through distinct mass lines.

Time-of-flight mass spectrometers offer high sensitivity, achieved through a robust ion-optical analyzer system, a wide dynamic range that enables precise measurement of isotope ratios, and a substantial mass range, often constrained only by the instrument's memory capacity. Similar to quadrupole mass spectrometers, time-of-flight mass spectrometers can utilize a variety of ionization sources. Furthermore, a significant benefit of time-of-flight mass spectrometers is their non-scanning operation, rendering them very well-suited for mission profiles involving the atmospheric descent of a Uranus probe. However, time-of-flight mass spectrometers have some drawbacks. They require fast electronics, which can be more complex to manage, and they produce data at a rapid rate, necessitating robust onboard data

processing to handle the large volume of information. Fortunately, space-rated high-speed Analog-to-Digital Converters (ADCs) with GSample/sec sampling rates are now available to support the needs of time-of-flight instruments. Additionally, space-rated high-speed Field-Programmable Gate Arrays (FPGAs) offer the processing power required to manage these high data rates, helping to mitigate this challenge to some extent. Despite these solutions, transmitting the large quantity of data produced by time-of-flight mass spectrometers to Earth remains a significant challenge.

Time-of-flight mass spectrometers have flown on Vega 1 and Vega 2 (ING; Curtis et al. 1987) to comet Halley and Venus, on BepiColombo (STROFIO; Orsini et al. 2010; Gurnee et al. 2012; Orsini et al. 2021) to Mercury, on Luna Resurs (NGMS; Wurz et al. 2012; Hofer et al. 2015; Fausch et al. 2018) to the Moon, on Rosetta (RTOF and COSAC; Balsiger et al. 1998; Scherer et al. 2006; Balsiger et al. 2007; Glassmeier et al. 2007; Goesmann et al. 2007, 2015) to comet Churyumov-Gerasimenko, and on JUICE (NIM; Barabash et al. 2013; Meyer et al. 2017; Föhn et al. 2021) and on Europa Clipper (MASPEX; Brockwell et al. 2016; Miller et al. 2022; Waite et al. 2024) to Jupiter's icy moons.

Ion Trap Mass Spectrometers: Ion trap mass spectrometers operate by capturing and manipulating ions through the application of three-dimensional quadrupolar electrodynamic fields generated by designated electrodes (Dawson 1979; Hughes et al. 2005). Ion traps are versatile instruments capable of capturing, confining, selectively ejecting, and isolating ions within their confines. To generate a mass spectrum, the radio-frequency voltages applied to the ion trap electrodes are scanned. This scanning process excites the ion trajectories of specific m/z ions, subsequently leading to their sequential ejection based on their mass-to-charge ratio (m/z). Ion traps exist in two primary forms: 2D and 3D ion traps. In 2D ion traps, ions are confined along a linear path, whereas 3D ion traps concentrate ions near the central point of the ion trap (also known as Quistors).

Ion trap mass spectrometers possess the ability to trap ions, allowing for their manipulation and selective analysis, as well as enabling ion accumulation to enhance the quality of statistical data. Ion trap mass spectrometers provide higher mass resolutions than quadrupole mass spectrometers, comparable to time-of-flight systems. In addition, ion trap mass spectrometers can be coupled to other mass spectrometers, making them especially useful in tandem mass spectrometry. Despite their relatively recent introduction to the mass spectrometry family, ion trap mass spectrometers have acquired flight heritage through their inclusion on Rosetta's Philae lander to comet 67P/Churyumov-Gerasimenko. The drawbacks of ion trap mass spectrometers include a somewhat intricate ionization process, limitations in dynamic range due to space charge effects in the ion trap (which limit isotope measurements), as well as sensitivity dependence on mass and instrument settings (Dawson 1979; Hughes et al. 2005). Additionally, they are susceptible to contamination of the ion-optical elements. Furthermore, akin to magnetic sector and quadrupole mass spectrometers, ion trap mass spectrometers operate as scanning instruments, which does not align optimally with the requirements of a Uranus probe.

Only one ion trap mass spectrometer has so far flown to space: the 3D ion trap instrument Ptolemy (Wright et al. (2007)) on the Philae lander of the Rosetta mission to comet 67P/Churyumov-Gerasimenko. Furthermore, a 2D ion trap mass spectrometer is part of the Mars Organic Molecule Analyzer (MOMA) experiment on the ExoMars rover scheduled to fly to Mars in 2028 (Goesmann et al. 2017).

Orbitrap Mass Spectrometers: Orbitrap mass spectrometers employ an electrostatic ion trap detection technique (Hu et al. 2005; Makarov et al. 2009), akin to ion cyclotron resonance

mass spectrometers. Within the Orbitrap, ions are confined by a quadrologarithmic electric potential, facilitating stable oscillations along the ion-optical axis as the ions orbit around a central spindle electrode. The frequency of these axial oscillations corresponds to the m/z values of the ions. As the ions undergo axial oscillations, they induce an image current on the outer electrodes of the Orbitrap. The induced image current is meticulously recorded as a time-domain signal by sensitive electronic detectors. Subsequently, this time-domain signal is transformed into a frequency spectrum using the Fourier transform, which can be converted to a mass spectrum, allowing for precise determination of the ions' masses and their relative abundances.

Orbitrap mass spectrometers offer exceptional mass resolution within the resources available in space flight. They can fairly easily switch between measuring positive or negative ions. Orbitraps do not need a dedicated detector, thereby mitigating the risk of detector degradation. However, they need highly sensitive pre-amplifiers to record the image current on the detection electrodes. Moreover, they demand very stringent high-voltage stability to achieve the high mass resolution and absolute mass determination, have limited ion-optical phase space, require intricate ion optics for efficient ion collection and transfer, and operate in phases that reduce overall usable measurement time. These instruments achieve high mass accuracy through mass calibration, but they are limited in dynamic range due to space charge effects and the Fourier transform principle (Grinfeld et al. 2019). One common issue with Orbitrap instruments is mass fractionation within the ion-optical system, which prepares the ions for analysis. As a result, extended integration times—often on the order of minutes—are required for accurate measurements. Isotope measurements with Orbitrap mass spectrometers have been reported only in a few instances, typically using laboratory-size high-end Orbitrap instruments (Hoegg et al. 2016,b; Eiler et al. 2017) or the very similar Fourier transform instruments (Spell et al. 1993; Barshick et al. 1998). For isotope analysis, it is typically necessary to isolate the isotope pair of interest in the Orbitrap analyzer and eject all other ions, further complicating the process. Given the limitations on a space instrument, isotope measurements on an Uranus probe are likely not feasible with an Orbitrap instrument.

No Orbitrap mass spectrometer has today flown on a space mission so far.

3.4 Detector

Mass spectrometrs employ a variety of detectors to capture and quantify ion signals, with some of them specialized for the specific needs of the mass analyzer. Commonly used detectors include Faraday cups and secondary electron multipliers. For the latter, there are channel electron multipliers, discrete dynode detectors, multichannel plates, and multisphere plates. Additional requirements may dictate the use of fast detectors (e.g., for time-of-flight mass spectrometers), imaging detectors (e.g., for magnetic sector systems), and solid-state detectors (e.g., for high-energy mass spectrometers like accelerator mass spectrometers). These detectors will be discussed briefly below while a comparison of their speed and gain, two of the most relevant parameters for mass spectrometers, is given in Fig. 3.

Faraday Cups: Faraday cup detectors function by having ion packets strike a metal surface, which then accumulates a small net charge as the ions neutralize on the detector's surface. Subsequently, the metal is systematically discharged through measurement electronics, allowing for the measurement of a small electric current directly proportional to the number of registered ions per second. These detectors provide high accuracy in signal quantification, as the measured current directly corresponds to the ion current. Faraday cups are robust and

exhibit no mass discrimination. However, they have very slow response times (ms to s time scale) and much lower sensitivity compared to other detectors. They often serve as reference detectors for calibration of mass spectrometers, mostly for magnetic sector instruments (e.g. Balsiger et al. 2007), recently also for a time-flight mass spectrometer (Waite et al. 2024), and possibly for quadrupole mass spectrometers.

Secondary Electron Multipliers: Secondary electron multipliers (SEMs) leverage the release of electrons from a solid surface when an energetic ion impacts it. In these detectors, this process triggers a cascade of secondary electrons, resulting in signal amplification with gains of up to 10^8. Electron multipliers come in both discrete (e.g., dynodes) and continuous variants (e.g., micro channel plates; MCPs), offering high sensitivity, even down to the level of single ion detection. They provide a linear response to the quantity of ions in a packet over a wide dynamic range and offer adjustable gain. However, at high extracted charges, such as high gain and/or high count rates, electron multipliers may deviate from linearity due to saturation effects. Additionally, they may exhibit slight mass discrimination effects stemming from the initial secondary electron release at the entrance electrode. Furthermore, these detectors require low ambient pressure environments (better than 10^{-5} mbar) due to their high-voltage operation. MCPs are often also used when fast detectors are required, as they can provide sub-nanosecond pulses for the detection of a single ion (e.g. Wurz and Gubler 1994, 1996). They are well-suited for capturing rapid processes and events in mass spectrometry experiments, providing high temporal resolution, and are typically needed for time-of-flight mass spectrometers (e.g. Scherer et al. 2006; Wurz et al. 2012). In addition, MCPs can be utilized as so-called imaging detectors, where not only the time but also the location of ion arrival on the detector surface is recorded by specialized anodes of the detector. These detectors are capable of detecting single particles and provide valuable spatial information alongside mass spectrometric data. For example, the magnetic sector mass spectrometer of the ROSINA experiment used an imaging detector (Berthelier et al. 2002).

Solid-State Detectors: Solid state detectors register single ions, and measure the ion's energy by collecting the charge carriers released by the ion in the semiconductor material placed between two electrodes. When ions strike the semiconductor, they create free electrons and electron holes. The number of electron-hole pairs produced is directly proportional to the energy of the ions. This leads to electrons moving from the valence band to the conduction band, creating an equal number of holes in the valence band. When an electric field is applied, electrons and holes move toward the respective electrodes, generating a measurable charge pulse in an external circuit. Since the energy required to create an electron-hole pair is constant, measuring the number of these pairs allows the energy of the ionizing radiation to be calculated. By analyzing these pulses, scientists can determine the mass-to-charge ratio, energy, and arrival time of the ions. Solid-state detectors, in addition to registering a particle, also measure its energy. This capability is valuable in accelerator mass spectrometers for resolving isobaric interferences, even at single-particle detection levels.

4 Synergies with Other Instruments

A mass spectrometer aboard a dedicated Uranus probe would enable the measurement of the planet's local chemical and isotope composition during its descent, aligning with the scientific inquiries outlined in Sect. 2. Note, that the mass spectrometer only provides information

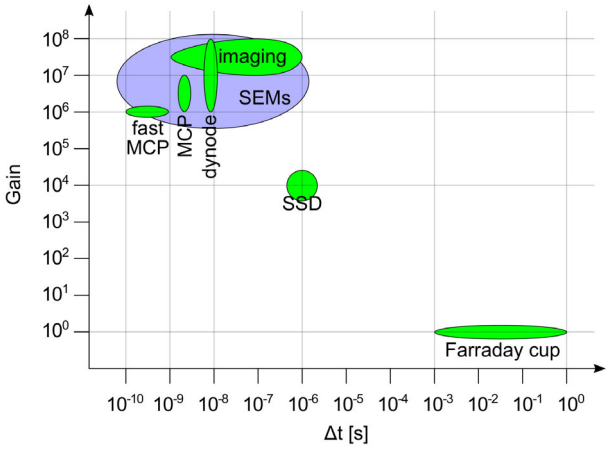

Fig. 3 Comparison between the speed and gain of different detector types. The green ovals denote approximate characteristic values for each type. Also shown is a group of the secondary electron multipliers (SEMs) in blue

on the upper part of the planet's atmosphere down to the operation altitude (actually, the operation pressure range) of the descending probe. Interpreting these measurements in relation to Uranus' formation, evolution, and internal structure necessitates elaborate models. Also, a good understanding of the atmosphere-interior interaction in Uranus is desirable.

In addition, it is important to recognize that a mass spectrometer experiment could greatly enhance its scientific value through collaboration with a diverse range of complementary instruments, facilitating a comprehensive study of the planet's atmosphere and composition. In this context, we suggest a suite of potential additional instrumentation for the probe. The proposed instrumentation is generally in line with the equipment suggested in the Decadal Survey (National Academies of Sciences, Engineering, and Medicine 2023), but it is slightly more comprehensive. In addition to the mass spectrometer, the Decadal Survey suggests including an atmospheric structure instrument, an ortho-para hydrogen sensor, and possibly an ultra-stable oscillator. However, it does not specifically call for other instruments like a nephelometer, a net-flux radiometer, a helium abundance detector, or a tunable laser spectrometer, which we propose including in our instrumentation suite.

In addition to the science questions a mass spectrometer can address independently, particularly concerning Uranus' origin, its synergy with other proposed instruments would help answer further questions, such as (i) what is the 3D atmospheric structure in the weather layer (with the atmospheric structure instrument, the H_2 ortho-para instrument, and the ultra-stable oscillator), (ii) what is the bulk composition and its depth dependence (with the ultra-stable oscillator), (iii) does Uranus have discrete layers or a fuzzy core and can this be tied to its formation and tilt (with the ultra-stable oscillator), (iv) what is the true rotation rate of Uranus, does it rotate uniformly, and how deep are the winds (with the ultra-stable oscillator), and (v) what dynamo process produces Uranus' complex magnetic field (with the ultra-stable oscillator). Furthermore, synergistic measurements between the mass spectrometer experiment and the H_2 ortho-para instrument could help further constrain the atmospheric circulation from the interior to the thermosphere and help answer the question of when, where, and how Uranus formed and how it evolved both thermally and spatially.

In a broader context, integrating the proposed instrumentation collaboratively aims to address key questions about Uranus' origin. It will explore issues like the planet's formation in the protosolar nebula, whether it migrated or exchanged positions with Neptune, and the possible impact of a giant collision in tilting Uranus and altering its interior structure. Beyond these formation questions, the instrumentation will also investigate ongoing processes,

such as heat and energy transport mechanisms, and examine how external factors affect the planet. Additionally, the proposed approach will contribute to a deeper understanding of the formation and evolution of ice giant-mass planets in exoplanetary systems, revealing interconnections between these processes and the broader universe.

Atmospheric Structure Instrument (ASI): The Atmospheric Science Instrument (ASI) is a versatile multi-sensor package designed to capture essential data as a probe descends through the atmosphere. Building upon the successful Huygens HASI instrument (Ferri et al. 2002; Fulchignoni et al. 1997, 2002), Ferri et al. (2020) advocates the inclusion of four crucial sensors within this package: a scientific accelerometer, a temperature sensor, a pressure profile instrument, and an atmospheric electrical package. The accelerometer incorporates a seismic mass that experiences displacement during the atmospheric descent. By detecting this displacement and applying corrective action, the accelerometer directly measures the probe's acceleration. Wire resistance thermometers are proposed to measure temperature variations. These sensors rely on changes in the resistance of a metallic wire as the temperature fluctuates, with comparison to a reference resistor powered by the pulsed current. Pressure measurement involves a sensor featuring a small vacuum chamber between two electrode plates. The external pressure determines the distance between these plates (Baratron capacitance manometers), facilitating accurate measurement of atmospheric pressure variations during descent. The atmospheric electrical package comprises a set of electrodes designed to assess a wide range of atmospheric electrical properties. It can measure atmospheric conductivity, both AC and DC electric fields, and monitor Schumann resonance. Schumann resonances are global electromagnetic resonances, generated and excited by lightning discharges inside the ionospheric cavity and might be used for constraining the uncertainty of volatiles of Uranus and Neptune. Additionally, it offers insights into electrical charges and fields. By integrating these sensors into the ASI, the instrument becomes a powerful tool for characterizing Uranus' atmosphere. It enables the study of atmospheric stability, dynamics, stratification, winds, waves, thermal tides, turbulence, condensation, aerosols, cloud layers, both saturated and unsaturated regions, stable and conditionally stable regions, moist convective processes, and electrical phenomena, including the potential detection of lightning (Ferri et al. 2020).

Ultra-Stable Oscillator or Doppler Wind Experiment: An ultra-stable oscillator or Doppler wind experiment serves as a valuable tool for gauging the altitude profile of zonal winds along the probe's descent trajectory. It provides insights into atmospheric turbulences, aerodynamic buffeting, and atmospheric convection and waves. This is achieved through Doppler tracking of the probe by the carrier spacecraft's radio subsystem, assuming that the probe, after the parachute deployment, moves in accordance with the winds and undergoes motions driven by atmospheric turbulence, aerodynamic buffeting, and atmospheric convection and waves. The characterization of these atmospheric phenomena is carried out by comparing the measured relay link frequencies to the expected relay frequencies between an ultra-stable oscillator situated on the probe and a counterpart ultra-stable oscillator located within the relay receiver on the carrier spacecraft.

Nephelometer: A nephelometer plays a pivotal role in providing valuable information about cloud locations and the characteristics of both liquid and solid particles, encompassing aerosols and haze particles. This is achieved by assessing the light-scattering properties exhibited by these particles. The process involves passive sampling of cloud and haze particles, which are subsequently exposed to a collimated beam of light. As the collimated light

encounters liquid and solid particles, it scatters in various directions, influenced by factors such as particle size, shape, and refractive index. Incorporated photo-detectors capture and measure the flux and polarization of the scattered light, allowing for a comprehensive characterization of the liquid and solid particles. In addition to its role in particle characterization, a nephelometer can contribute to measuring vertical heat fluxes resulting from latent heat. Furthermore, it serves as an invaluable *in situ* reference for remote sensing applications, mitigating the significant ambiguity often encountered in remote sensing retrievals.

H_2 Ortho-Para Instrument: An H_2 ortho-para instrument serves as a valuable tool for discerning the proton spin type of encountered hydrogen molecules during a probe's descent into the atmosphere. Specifically, it identifies whether the hydrogen molecules are in a parallel (ortho-hydrogen) or anti-parallel (para-hydrogen) configuration. The ratio of these configurations offers insights into the ambient temperature and the adiabatic lapse rate if the gases are allowed to equilibrate over time. In cases where equilibrium times are sufficiently long, this ratio can also be employed to trace the past environmental conditions of a given air parcel. A suitable instrument could be a successor of the sonic anemometer initially developed for use on Mars' surface (Banfield et al. 2016). It utilizes broadband capacitive transducers to precisely measure the acoustic travel time of a coded signal through the atmosphere in two opposing directions. To determine the ortho-para fraction accurately, these travel time measurements must be coupled with kinetic temperature measurements. The H_2 ortho-para instrument plays a crucial role in providing essential information for the correct interpretation of various atmospheric aspects on Uranus. This includes the thermal profile and stability, density structure, aerosol layering, net fluxes, and vertical motions within the planet's atmosphere.

Net-Flux Radiometer: A net-flux radiometer serves as a vital instrument for quantifying both the net and upward radiation flux within the atmosphere, thus enabling the determination of the radiative (cooling) component of the atmospheric energy budget. This instrument comprises an optical head equipped with detectors that observe a portion of the local atmosphere through a diamond window. Behind this window, multiple detectors are strategically placed, each equipped with filters covering a range of wavelengths from visible to infrared. Aslam et al. (2020) proposes a net-flux radiometer that incorporates seven detectors, including one designed to capture all scattered solar radiation and two specialized detectors that capture progressively more absorbed radiation due to gaseous methane. The net-flux radiometer plays a pivotal role in observing fluctuations in the net radiation flux, offering insights into the driving forces behind atmospheric motions by assessing whether and to what extent a particular layer is radiatively heated or cooled. Additionally, it can identify regions where the atmosphere absorbs radiation relatively strongly, and the magnitude of this absorption can be correlated with temperature and pressure data from the ASI and particle backscatter measurements from the nephelometer. Overall, the scientific objective of the net-flux radiometer is to enhance our understanding of several key aspects of Uranus' atmosphere, including its heat balance, sources and sinks of planetary radiation, regions of solar energy deposition, as well as insights into atmospheric composition and cloud layers.

Helium Abundance Detector: A Helium abundance detector can determine the He/H_2 ratio with high accuracy. This is accomplished by measuring the refractive index of the atmosphere, which is a function of the composition of the sampled gas. Assuming that Uranus' upper atmosphere consists mostly of H_2 and He, the refractive index is for the most part a direct measure of the He/H_2 ratio. The refractive index can be measured by a two-beam

interferometer, where the difference in the optical path between one beam passing through a reference gas and another beam passing through atmospheric gas gives the refractive index between the two gasses (Von Zahn and Hunten 1992).

Tunable Laser Spectrometer: A Tunable Laser Spectrometer (TLS) enhances the mass spectrometry measurements, and would provide redundancy for isotope measurements, by offering precise isotope measurements for several elements, such as D/H, $^{13}C/^{12}C$, $^{18}O/^{16}O$, and $^{17}O/^{16}O$, contingent upon the chosen laser systems. The TLS utilizes ultra-high spectral resolution (0.0005 cm^{-1}) tunable laser absorption spectroscopy within the near-infrared (IR) to mid-IR spectral range. A TLS is an integral component of the SAM instrument onboard the NASA Curiosity Rover (Webster and Mahaffy 2011). This instrument was employed to determine isotope ratios, including D/H and $^{18}O/^{16}O$ in water, as well as $^{13}C/^{12}C$, $^{18}O/^{16}O$, $^{17}O/^{16}O$, and $^{13}C^{18}O/^{12}C^{16}O$ in carbon dioxide within the Martian atmosphere (Webster et al. 2013). A TLS is a valuable addition to a mass spectrometer, offering two significant benefits: it can deliver more precise measurements of specific isotope ratios than a mass spectrometer, and it provides a means of redundancy and verification for the isotope ratio data obtained from the mass spectrometer. However, the TLS operation is completely independent of the mass spectrometer operation.

5 Proposed Implementation

As explained in the science motivation in Sect. 2, the mass spectrometer experiment for a Uranus probe must be capable of determining the chemical composition of Uranus' atmosphere, including the abundance of hydrogen and helium. It must also conduct isotope analyses of key elements and measure the presence of noble gases along with their isotopic compositions. These tasks must be completed within a highly constrained mission profile, requiring efficient data collection and analysis.

In the following section, we introduce a comprehensive mass spectrometer experiment designed to address all the scientific inquiries outlined in this paper. This experiment is a revised version of the mass spectrometer experiment already presented in Vorburger et al. (2020). Toward the conclusion of this section, we provide a detailed list of the projected species-dependent performance of this system.

5.1 Mass Spectrometer Experiment

As discussed in Sect. 3.3 there are several choices for the mass analyzer. Given that on an atmospheric probe, the time available for measurements during the descent is about one hour, a non-scanning instrument is preferred. The requirements for chemical separation are moderate because the chemistry in Uranus' atmosphere is simple as reviewed in (Mousis et al. 2018, 2022). However, the requirements for sensitivity are high because the sparse noble gases shall be measured, including the abundances of their isotopes. Therefore we decided on a time-of-flight mass spectrometer with an MCP detector system, which is discussed in detail below. Time-of-flight mass spectrometers are highly reliable while simple to operate, which is of advantage for a short mission in a challenging environment at fully autonomous operation.

Figure 4 illustrates the proposed configuration of the mass spectrometer experiment for a Uranus probe. The gas inlet, located at the bottom left (Break-off valve inlet), connects to the gas outlet, positioned at the top left (Break-off valve outlet). During the launch and

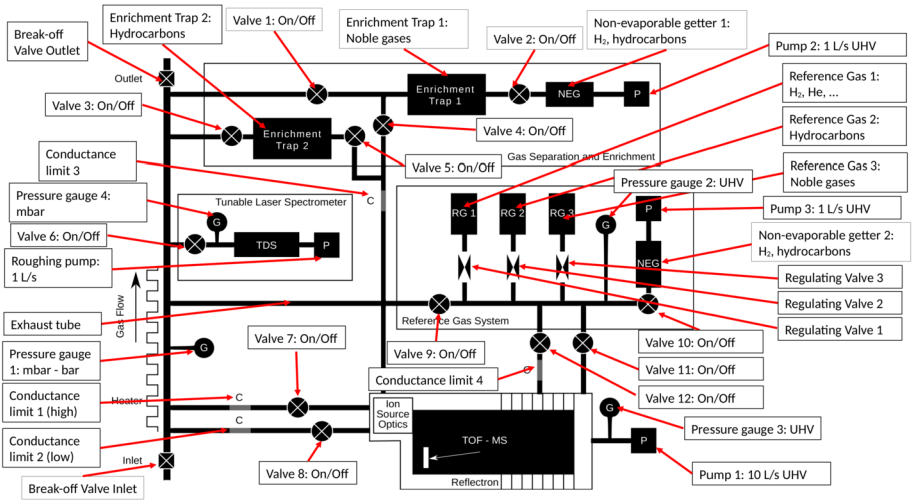

Fig. 4 Proposed mass spectrometer experiment implementation for a Uranus atmospheric probe

cruise phases, both the inlet and outlet remain hermetically sealed by a valve. These valves are opened only when the probe reaches a pressure of approximately $\sim 1 \cdot 10^{-7}$ mbar. After the valves have been opened, gas continuously streams from the inlet to the outlet, ensuring that measurements consistently represent the local atmospheric conditions.

To maintain functionality and prevent gas condensation on inner tube walls, a heater can be applied to the tube connecting the inlet and outlet. In addition, this heater also allows the measurement of simple aerosol particles that might have entered the inlet and that stick to the inner walls.

As gas continuously flows from the inlet to the outlet, a portion of it can be diverted to either the mass spectrometer system or the TLS. The diversion to the mass spectrometer system can be managed using two valves (Valve 7 and 8) and two tubes with distinct conductances (Conductance limits 1 and 2), each optimized for measurements within different atmospheric pressure ranges. The mass spectrometer is equipped with a pressure gauge (Pressure gauge 3) and a pump (Pump 1) to remove the analyzed gas. Further down the gas flow path between the inlet and outlet, a second pressure gauge (Pressure gauge 1) provides the absolute atmospheric pressure necessary for absolute calibration.

The TLS measurement is started by opening the dedicated valve (Valve 6) until the operating pressure of approximately $\sim$10 mbar is reached in the TLS cavity when the valve is closed, which is controlled by a dedicated pressure gauge (Pressure gauge 4) to ensure compliance with this requirement. Then the actual TLS measurement commences, and upon its completion, the TLS cavity is evacuated by a dedicated pump (Roughing pump) to prepare for the next measurement cycle. A TLS instrument has not been employed for the large pressure range foreseen for an atmospheric probe, thus its design might be more complicated than what is envisioned at present (see Fig. 4).

Located farther along the gas flow path, a Separation and Enrichment system is positioned. Before atmospheric measurements commence, this system can be evacuated through two valves (Valves 1 and 3). One trap (Enrichment trap 1) is designated for noble gas measurements, while the other trap (Enrichment trap 2) is intended for hydrocarbon measurements. The operational timeline envisions that during normal operation (direct inlet to the

mass spectrometer), the enrichment cells accumulate gases, enriching the desired rare gases (i.e., noble gases and hydrocarbons). Periodically, the direct inlet to the mass spectrometer is paused (by closing Valves 7 and 8) to allow the feeding of the enriched gases into the mass spectrometer system for analysis instead (by opening Valves 4 and 5). The enrichment cells are connected to the mass spectrometer with a tube with a specified conductance limit (Conductance limit 3), ensuring that the pressure in the mass spectrometer does not drastically change between different measurement modes (i.e., nominal measurement and measurement of the enriched gases). The enrichment trap accumulating noble gases (Enrichment trap 1) also connects to a non-evaporable getter (Non-evaporable getter 1) via a third valve (Valve 2) to remove H_2 and hydrocarbons, potentially interfering molecules with the noble gas measurements. A pump (Pump 2) removes gases collected by the non-evaporable getter.

To calibrate the mass spectrometer in flight and enhance the accuracy of crucial measurements, a reference gas system is integrated. When the Uranus Orbiter and Probe enters the Uranus system, once the inlet and outlet valves have been broken off, any gases that have accumulated in the reference gas system during the multi-year cruise period will be evacuated using a designated valve (Valve 9). After this initial evacuation, Valve 9 will remain closed, and for any further reference gas system clearings Valve 10 will be used. The mass spectrometer experiment will be calibrated before the atmospheric measurements and immediately after opening the break-off valves of the inlet and outlet. Three gases are allocated for a mass spectrometer designed for a Uranus probe: one containing H_2 and Helium as a reference, one containing hydrocarbons, and one featuring a specific blend of noble gases. Selection among these reference gases can be accomplished by opening one of three variable leak-regulating valves (Regulating Valves 1 through 3, which normally seal the reference gas reservoirs). The chosen reference gas is then introduced via a valve (Valve 12) and a tube with defined conductance (Conductance limit 4) into the mass spectrometer system. The Reference Gas System also connects to the mass spectrometer system through a second valve (Valve 11), which serves as a higher conductance pathway to Pump 1 for purging any remaining gases from the manifold when transitioning between the three reference gases. Moreover, the Reference Gas System includes a non-evaporable getter (Non-evaporable getter 2) to eliminate any residual H_2 and hydrocarbons via a valve (Valve 10). Finally, a third pump (Pump 3) evacuates any remaining gases from the Reference Gas System, while a pressure gauge (Pressure gauge 2) monitors and maintains the desired pressure range within the Reference Gas System. After analyzing the reference gases, all valves connecting the reference gas system to the mass spectrometer are closed, and the nominal operation, as described above, commences.

The estimated resources needed for such a Mass Spectrometer experiment for the atmospheric probe are a weight of 11 kg, a size 24.5 x 14.5 x 22.9 cm^3, and an average power requirement of about 28 W for full operation. These estimates are based on earlier designs of mass spectrometers for space research (Balsiger et al. 2007; Wurz et al. 2012; Fausch et al. 2018; Föhn et al. 2021) and the Gallileo Probe mass spectrometer (Niemann et al. 1992). The proposed design's complexity is evident, incorporating 12 on/off valves, three regulating valves, and four pumps. This complexity arises because the mass spectrometer must operate in a high-pressure regime, which necessitates a dedicated vacuum system. Additionally, to ensure high accuracy—especially considering the low mixing ratios of some species—two enrichment systems and a reference gas system are required. To put this in perspective, the Galileo probe, which also used two enrichment systems but lacked a reference gas system, employed 13 micro-valves and one ion pump Niemann et al. (1992). The MAss Spectrometer for Planetary EXploration (MASPEX), aboard the Europa Clipper, includes a calibration gas system and a cryotrap but isn't designed for high-pressure environments.

Table 4 Sample operation sequence of mass spectrometer experiment during the descent through Uranus atmosphere. Altitudes are given in reference to the 1 bar level

Phase	Altitude from–to [km]	Pressure from–to [mbar]	Time from–to [sec]	Speed [m/s]	Integration time [sec]	Vertical resolution [km]	Number of mass spectra
0	1500–450	$1.0 \cdot 10^{-7}$–$1.0 \cdot 10^{-4}$	(−414.18)–0	2535	30	75.00	14
1	450–15	$1.0 \cdot 10^{-4}$–$4.0 \cdot 10^{+2}$	0–172	2529	15	36.25	12
2	15–14	$4.0 \cdot 10^{+2}$–$4.2 \cdot 10^{+2}$	172–183	91	12	1.05	1
3	14–10	$4.2 \cdot 10^{+2}$–$5.0 \cdot 10^{+2}$	183–235	77	10	0.81	5
4	10–(−13)	$5.0 \cdot 10^{+2}$–$1.6 \cdot 10^{+3}$	235–581	66	10	0.68	34
5	(−13)–(−99)	$1.6 \cdot 10^{+3}$–$1.0 \cdot 10^{+4}$	581–2101	57	15	0.85	101
6	(−99)–(−140)	$1.0 \cdot 10^{+4}$–$2.4 \cdot 10^{+4}$	2101–3684	26	20	0.51	80

This spectrometer uses seven valves and two pumps Waite et al. (2024). The proposed design's complexity is, therefore, comparable to these existing systems. The design details of MASPEX, particularly its valves and pumps, could serve as a useful reference point for this new system Waite et al. (2024).

The Galileo atmospheric probe had a mass spectrometer experiment (Niemann et al. 1992) and in addition a Helium abundance detector (HAD) for the accurate measurement of the He/H_2 ratio Von Zahn and Hunten (1992). For the Uranus probe, the addition of a HAD for the accurate He/H_2 measurement is not necessary anymore, resulting in a mass saving of approximately 1.4 kg—the equivalent mass of the HAD utilized on Galileo (Von Zahn and Hunten 1992). This measurement can be done with the mass spectrometer experiment as well for two reasons. First, a dedicated He/H_2 reference gas mixture is part of the proposed mass spectrometer experiment (see Fig. 4) that provides a direct reference for this important measurement. Second, in the forty years since the Galileo mission the technology of mass spectrometers advanced significantly, i.e., the mass resolution of the present instrument is about 10 times that of the Galileo mission (Niemann et al. 1992), the sensitivity increased by about three orders of magnitude (Niemann et al. 1992), and full mass spectra are measured at a cadence of 20 kHz (Wurz et al. 2012). Histogrammed over the proposed integration periods of 10 to 30 seconds, the mass spectrometer would deliver complete mass spectra with altitude resolutions in the kilometer range (refer to Table 4).

Table 5 outlines the anticipated performance of the proposed mass spectrometer experiment during the descent through Uranus' atmosphere. The table is constructed based on estimated abundances of various species (as indicated) and follows an operation sequence as detailed in Table 4. Apart from the complex hydrocarbons only present in the photochemical layer, the mixing ratio of the different species is assumed to be constant with depth. The expected accuracy of the mass spectrometric measurements is calculated based on the performance of the mass spectrometer for the lunar exosphere (Wurz et al. 2012), using an integration time for the mass spectra of 11 s. Results are presented for the major chemical species, noble gases, and some isotope ratios of interest. For the photolytic layer in the upper atmosphere, where a lot of hydrocarbon compounds are expected, we present the calculation only for acetylene and benzene, but all the other hydrocarbons will be recorded with comparable performance. Also, the use of the enrichment cells and the reference gases is indicated in Table 5. In most cases, the expected accuracies surpass the minimum requirements outlined in the (National Academies of Sciences, Engineering, and Medicine 2023). According to this source, the following accuracy thresholds are stipulated: 5% for noble gas

Table 5 Estimated expected accuracies for measurements for selected species for the mass spectrometry experiment shown in Fig. 4 for a sample operation sequence (presented in Table 4). This estimate assumes the sensitivity of the mass spectrometer for the lunar exosphere (Wurz et al. 2012), an integration time for the mass spectra of 11 s (except for Ne, Ar, Kr, and Xe, where an integration time of 400 s is used), chemical abundances as they are known for Uranus and otherwise from Jupiter, and terrestrial isotope abundances. Measurements are performed in different modes: "L" for low sensitivity mode, "H" for high sensitivity mode, "RGx" for using reference gas x for calibration, "ETx" for using enrichment trap x for sample collection. Based on National Academies of Sciences, Engineering, and Medicine (2023), the required accuracies are 5% for noble gases, 5% for the isotopes of He and Xe, and 20% for more abundant molecules

Species	mode	rel. abundance	exp. accuracy	isotope ratio	exp. accuracy
H_2	L	1	5.00%	HD/H_2	0.89%
He	L	0.176	5.00%	$^3He/^4He$	1.42%
He/H_2	L, RG1	0.176	1.50%		
CH_4	L, H	$5.33{\cdot}10^{-3}$	5.00%	$^{12}C/^{13}C$	0.20%
NH_3	L, H	$4.54{\cdot}10^{-4}$	5.00%	$^{14}N/^{15}N$	1.04%
H_2O at 2 bar	H	$2.30{\cdot}10^{-7}$	5.74%		
H_2O at 10 bar	H	$2.00{\cdot}10^{-4}$	5.00%	$^{16}O/^{17}O$	5.02%
				$^{16}O/^{18}O$	2.10%
H_2S	L,H	$3.76{\cdot}10^{-4}$	5.00%		
CO	H	$1.00{\cdot}10^{-9}$	110.50%		
CO_2	H	$3.40{\cdot}10^{-10}$	308.60%		
PH_3	H	$7.28{\cdot}10^{-6}$	5.02%		
AsH_3	H	$2.64{\cdot}10^{-9}$	46.80%		
GeH_4	H	$3.50{\cdot}10^{-10}$	300.00%		
C_2H_2	H, ET2, RG2	$4.00{\cdot}10^{-6}$	5.04%		
C_2H_6	H, ET2, RG2	$4.50{\cdot}10^{-6}$	5.04%		
Ne	H	$2.48{\cdot}10^{-5}$	5.00%	$^{20}Ne/^{22}Ne$	0.18%
Ne/He	H, ET1, RG3	$1.41{\cdot}10^{-4}$	1.52%	$^{20}Ne/^{21}Ne$	0.88%
				$^{21}Ne/^{22}Ne$	0.89%
Ar	H	$1.82{\cdot}10^{-5}$	5.00%		
Ar/He	H, ET1, RG3	$1.21{\cdot}10^{-2}$	1.50%	$^{36}Ar/^{38}Ar$	0.11%
Kr	H	$9.30{\cdot}10^{-9}$	5.76%		
Kr/He	H, ET1, RG3	$1.16{\cdot}10^{-5}$	2.47%	$^{78}Kr/Kr_{tot}$	11.53%
				$^{80}Kr/Kr_{tot}$	11.82%
				$^{82}Kr/Kr_{tot}$	2.82%
				$^{83}Kr/Kr_{tot}$	1.43%
				$^{84}Kr/Kr_{tot}$	1.13%
				$^{86}Kr/Kr_{tot}$	0.69%
Xe	H	$8.90{\cdot}10^{-10}$	20.62%		
Xe/He	H, ET1, RG3	$1.82{\cdot}10^{-6}$	6.89%	$^{124}Xe/Xe_{tot}$	415.6%
				$^{126}Xe/Xe_{tot}$	415.6%
				$^{128}Xe/Xe_{tot}$	20.8%
				$^{129}Xe/Xe_{tot}$	2.9%
				$^{130}Xe/Xe_{tot}$	10.6%
				$^{131}Xe/Xe_{tot}$	3.2%
				$^{132}Xe/Xe_{tot}$	2.9%
				$^{134}Xe/Xe_{tot}$	5.0%
				$^{136}Xe/Xe_{tot}$	5.7%

mixing ratios, 5% for the isotope ratios of helium and xenon, and 20% for more prevalent species such as CH_4, H_2S, C_2H_2, and C_2H_6. Of course, for species at very low abundances, the accuracies decrease, for example, CO_2, which can only be measured with an accuracy within a factor of 3. Further challenges arise with the mixing and isotope ratios of the heavy noble gases, Kr and Xe, due to their extremely low abundance, assuming values based on measurements from Jupiter (see Table 1). To address these challenges, the integration time was extended from 11 seconds — typically used for measuring other species — to 400 seconds, enhancing the accuracy of isotope measurements by a factor of 6. This increased integration time met the required accuracy standards and doubled the improvement over the Galileo mission, which had an integration time of 434 seconds (Niemann et al. 1998). For the accuracy calculations, the noble gas abundances from Jupiter were utilized (see Table 1). However, if noble gases are enriched by a factor of 20 to 120 on Uranus (see Fig. 2), translating to an enrichment of 7 to 40 times the Jupiter values, the accuracy of noble gas isotope measurements will improve accordingly.

5.2 Atmospheric Probe

There are multiple design possibilities for a flagship NASA mission to Uranus. If the European Space Agency (ESA) provides a budget similar to that of M-class missions (approximately 500 million of 2023 euros), a probe design akin to the Galileo probe can be developed. This concept is quite similar to the Hera Saturn probe proposal submitted to ESA's previous M4 and M5 calls that includes a science payload comprising five instruments (a net flux radiometer, a nephelometer, a radio science instrument, an atmospheric structure instrument, and a mass spectrometer including a tunable laser spectrometer) and weighs about 300 kg (Mousis et al. 2016). An alternative scenario could involve supplying a probe module to NASA by a consortium of European Union countries, independently of ESA. Internal studies by ArianeGroup suggest that a simpler probe concept with a basic payload, consisting of a mass spectrometer and an atmospheric structure instrument, could weigh as little as 70 kg (Mousis et al. 2024). This streamlined probe design could stay within a 100-150 million euro budget, excluding instruments.

Uranus is the only outer planet in the solar system that is in approximate equilibrium with solar insolation (Pearl et al. 1990; Pearl and Conrath 1991), which will be investigated from the orbiting spacecraft. One of the numerous methods proposed for achieving this thermal equilibrium (Cohen et al. 2022) is atmospheric phenomena (Gierasch and Conrath 1987; Kurosaki and Ikoma 2017), which can be addressed by the atmospheric probe measurements. Many atmospheric processes in the atmosphere cause downward and upward radiation of energy, the former by e.g., solar insolation and the latter by e.g., thermal radiation, cumulus convection, and vertically propagating waves. The atmospheric processes provide local perturbations that shape atmospheric features such as cloud bands and vortices. Furthermore, the total upward heat flux in the atmosphere is the sum of all local processes. The connection between local atmospheric events and the global energy balance (e.g., Helled and Fortney (2020) and references therein) remains an outstanding question and will be addressed by having local measurements by the atmospheric probe and global measurements by the orbiting spacecraft.

A crucial aspect to address concerning the atmospheric probe is the selection of the entry and descent point within Uranus' atmosphere. This decision involves pinpointing the precise location where the atmospheric probe will enter Uranus' atmosphere. Several factors and limitations come into play, including the trajectory of the main spacecraft (the orbiter responsible for deploying the probe), communication constraints between the descending

probe and the main spacecraft, and timing considerations. In the following, we give some considerations on selecting the entry point location.

Probe Entrance at Lower Latitudes: Entering at lower latitudes, at a quiet location (e.g. without any visible small-scale structure in the atmosphere indicative of turbulence) might allow for a representative measurement of the global composition and structure of Uranus' atmosphere. What remains to be decided is whether it is favorable to select an entry location near the equator, within 20°S and 20°N where the zonal flow is retrograde, or an entry location at higher latitudes, with fast prograde zonal flows (Soyuer et al. 2020). The retrograde winds can reach up to 100 km/s, whereas the prograde winds even reach up to 200 km/s. Understanding atmospheric circulations, such as atmospheric banding, is pivotal for comprehending vertical heat transport, maintaining energy balance, and advancing atmospheric dynamic modeling. Furthermore, insights into these circulations help elucidate their extension into the planet's interior. This simple structure of the zonal wind is in strong contrast to the finely banded winds on Jupiter and Saturn. An original launch date of the Uranus Orbiter and Probe of 2031 was foreseen, allowing an arrival at Uranus in 2044 with a gravity assist at Jupiter (National Academies of Sciences, Engineering, and Medicine 2023). Currently, however, a later launch in the mid to late 2030s is more likely, shifting the arrival to nearly 2050. Thus, Uranus would be illuminated by the Sun roughly sideways and the northern and southern hemispheres would receive similar Sun illumination.

Polar Entrance: Arriving at Uranus when it is oriented sideways with respect to the Sun allows access by the atmospheric probe even to the poles, as Uranus' rotation axis is close to the ecliptic plane. With a Uranus Orbiter and Probe arrival around 2045, the north pole will have come out of a long winter, and the south pole will experience a long summer. There are reasons to prefer either pole for placing the atmospheric probe, depending on the year of arrival, since seasonal changes have been suggested to cause hemispheric asymmetry of the atmosphere (Sromovsky et al. 2014) (Karkoschka 2015). Around the poles, a depletion of the gases CH_4, H_2S, and NH_3 is observed down to the NH_4SH cloud layer (Sromovsky et al. 2015; Molter et al. 2021). Based on this depletion it is suggested that Uranus has a single deep circulation cell in each hemisphere, or a three-layer hemispheric convection cell, in which air rises from the deep atmosphere at low latitudes, clouds condense out, and dry air is transported to high latitudes, with downwelling at the polar vortex (Sromovsky et al. 2015). A depletion of some atmospheric compounds makes a descent into the polar atmosphere less favorable.

Cloud Locations: There are places with clouds running at constant latitudes, places with individual clouds, and cloud-free areas. Clouds are condensed volatiles, thus their composition and formation have an impact on the energy budget of the atmosphere, and thus their observation and characterization are of great interest. The cloud features range from small to large, from dim and diffuse to sharp and bright, and from rapidly evolving systems to stable features that last for years. Long and narrow complexes of cloud features are observed in the northern hemisphere, e.g. the 29,000-km-long complex of clouds that dissipated completely over the span of a month. In the three-layer convection cell model, clouds form in the upwelling regions of the atmosphere at low latitudes and the dry air continues to higher latitudes and the poles where it descends (Sromovsky et al. 2015; Cohen et al. 2022). In the upwelling regions, NH_4SH clouds are expected around 10 bars, H_2S clouds at about 1.5 bars, and CH_4 clouds around 1 bar (Cohen et al. 2022), which are all within reach considering a descent of the atmospheric probe to at least 20 bars, like the Galileo probe. So far,

the composition and location of the cloud layers remain unclear, but an atmospheric probe should greatly advance our understanding of clouds. As the probe descends into a pressure region corresponding to the upper levels of a cloud, the mass spectrometer is expected to detect a sharp increase in gases that have condensed to form the cloud. This sudden shift in atmospheric conditions also raises the risk of ice particles accumulating or droplets condensing in the gas flow path of the mass spectrometer. To mitigate these risks, starting at a few hundred mbar, the mass spectrometer will be periodically baked-out at regular intervals.

Dark Spot: There are singular locations observed on Uranus' surface that might be interesting for an investigation by an atmospheric probe. Because the molecular weight of condensable species is heavier than the dominant hydrogen-helium atmosphere, moist convection is generally inhibited, i.e., moisture tends to sink instead of rising. However, convection tends to happen in episodic bursts or storms, which are regularly observed (Cohen et al. 2022, and references therein) to raise material to higher altitudes in the atmosphere. The darkening, or the opacity change, described by Cohen et al. (2022) was suggested to be the result of a mixture of H_2S ice and photochemically produced haze related to a vortex (Irwin et al. 2022). The large, longer-lived clouds may be underpinned by giant hurricane-like vortices, as were seen on Neptune. An example is the great dark spot (Hammel et al., 2009), an anticyclonic storm located in the northern hemisphere at mid-latitudes (27°N), with an elongated shape that measures 1,700 km by 3,000 km. The great dark spot appears dark at visible wavelengths but bright at near-IR wavelengths. A storm might possibly provide upwelling from material from further inside, from depths that are not accessible by an atmospheric probe. The development of a dark spot may be a signal of the changing seasons along Uranus' orbit, e.g., in the case of the great dark spot of the oncoming Uranian northern spring. Upwellings from the interior, like the plume upwelling that was observed in the NH_3 data of Jupiter, showed that material from a depth of more than 60 bars rose to the 1 bar level without condensation (Bolton et al. 2017). At present, we do not know if the upwelling on Uranus would be of similar scale, i.e., if it reaches into the range of the atmospheric probe, but if so it would allow for detailed investigation of material from further down.

5.3 Atmospheric Orbiter: Complement of Probe Measurements

An orbiter of Uranus, as is foreseen in the Uranus Orbiter and Probe mission in the 2022 decadal survey (National Academies of Sciences, Engineering, and Medicine 2023), will, among other scientific investigations, provide complementary information about the atmosphere via remote sensing. The atmospheric measurements on the orbiter would, for example, be mapping the visible surface of Uranus (see Fig. 1), tracking storms, clouds, and eddies in reflected sunlight, and mapping key volatile species and abundances of hydrocarbons in the photolysis layer in the upper atmosphere. The orbiter measurements will provide us with the opportunity to contextualize the entry location of the atmospheric probe on a global scale. This includes assessing whether the probe's entry point aligns with a distinct atmospheric feature, gaining insights into the presence and characteristics of clouds and hazes at the entry site, and monitoring their temporal evolution during orbital observations. Additionally, these measurements will facilitate the study of various atmospheric phenomena, such as convection, upward and downward energy flow, and atmospheric wave activity. Such investigations will deepen our understanding of how these processes shape prominent atmospheric features like cloud bands and vortices. In addition, microwave observations might probe deep inside the atmosphere even below the reaches of an atmospheric probe, e.g., for H_2S (Molter et al. 2021) or for NH_3 at Jupiter (Bolton et al. 2017; see also Fig. 1).

5.4 Gravity Measurements

Last, but not least, measuring Uranus' gravitational field to higher accuracy via Doppler tracking would provide key constraints on Uranus' density profile, and therefore its composition and internal structure (e.g. Helled et al. 2020). Interior models of Uranus that fit the gravity data can be further constrained using the atmospheric measurements (with the requirement to reproduce the observed atmospheric metallicity). Updated interior models of Uranus together with accurate measurements of the atmospheric compositions and the different isotope ratios can then be used to reveal new information on Uranus' origin and long-term evolution.

Finally, accurate determination of Uranus' gravity field and the detection of odd harmonics can be used to constrain the depth of the winds in Uranus Kaspi et al. (2013), Soyuer and Helled (2021), Soyuer et al. (2023). This in return is not only important for understanding Uranus' atmosphere dynamics and the mechanisms that lead to the wind decay (e.g. Soyuer et al. 2020) but also for further constraining Uranus' internal structure Neuenschwander et al. (2024).

6 Conclusion

Several probe designs can be envisaged for a NASA-led flagship mission toward Uranus. Assuming ESA provides a budget equivalent to the one attributed to M-class missions (∼500 million of 2023 euros), a probe design close to the one of the Galileo probe can be envisaged. Such a probe design would be quite similar to the Hera Saturn probe proposal submitted to ESA's previous M4 and M5 calls that includes a science payload comprising five instruments (a net flux radiometer, a nephelometer, a radio science instrument, an atmospheric structure instrument, and a mass spectrometer including a tunable laser spectrometer) and weighs about 300 kg (Mousis et al. 2016). Another end-member scenario would correspond to the case where the probe module is only supplied to NASA by a consortium of several EU countries, independently of ESA. Internal studies led by ArianeGroup suggest that a probe concept containing as a minimum payload a Mass Spectrometer with an Atmospheric Structure Instrument could reach a mass as low as ∼70 kg (Mousis et al. 2024). Such a minimum probe design could remain in the 100–150 million euros cost cap, instruments excluded.

In this paper, we have conducted a review of the scientific objectives inherent to a Uranus probe. Our focus has centered on the chemical composition of Uranus' atmosphere, a pivotal aspect for comprehending the planet's origin, evolutionary processes, and the unique characteristics that distinguish it from other celestial bodies within our solar system.

Figure 1 provides a visualization of the informational depth achieved by various remote sensing techniques. It illuminates how an *in situ* probe has the potential to overcome the limitations posed by these techniques, with the notable exception of microwave measurements, which can delve deeply into Uranus' atmosphere but require model-dependent interpretations for a comprehensive understanding.

Furthermore, Fig. 2 and Tables 1 and 2 serve as powerful visual aids, emphasizing the substantial gaps in our current knowledge regarding the chemical composition of the ice giants, and the drastic knowledge increase one gains from a single entry probe as we had for Jupiter.

The mass spectrometry experiment assumes a pivotal role in meeting the critical scientific prerequisites of the Uranus atmospheric probe, much as it did for the Galileo probe's mass spectrometer during its mission to Jupiter (Niemann et al. 1992). Mass spectrometry

represents a well-established and widely recognized tool for conducting compositional analyses. In this paper, we conducted a concise evaluation of various mass spectrometer types relevant to potential implementation on an atmospheric probe. Table 3 lists the pros and cons of the major mass spectrometer types in view of an application on a Uranus probe.

Furthermore, we introduced a proposed implementation, which not only draws from the flight heritage of the Galileo probe but also capitalizes on advancements in technology that have transpired since the Galileo mission. A schematic of the proposed implementation is shown in Fig. 4, while the proposed sample operation sequence and the associated experiment measurement accuracies are presented in Tables 4 and 5, respectively. The suggested mass spectrometer experiment demonstrates capabilities surpassing those of the Galileo probe, all the while remaining feasible within the tight resource constraints associated with a Uranus probe.

Finally, we introduce several instruments slated for inclusion on the probe that promise to offer valuable synergies with the mass spectrometer experiment. These instruments encompass an atmospheric structure instrument, an ultra-stable oscillator or Doppler wind measurement device, a nephelometer, an H_2 ortho-para instrument, a net-flux radiometer, a tunable laser spectrometer, and a helium abundance detector. Furthermore, we delve into critical considerations regarding the probe's entry phase and explore the potential contributions that an orbiter could make to enhance the quality and scope of probe measurements, while exploring the prospects for establishing collaborative partnerships between NASA and ESA to ensure the successful realization of this groundbreaking probe.

Acknowledgements A. Vorburger and P. Wurz gratefully acknowledge the financial support by the Swiss National Science Foundation. O. Mousis acknowledges support from CNES and the Programme National de Planétologie (PNP) of CNRS/INSU. A part of the project leading to this publication has received funding from the Excellence Initiative of Aix-Marseille Université–A*Midex, a French "Investissements d'Avenir program" AMX-21-IET-018. This research holds as part of the project FACOM (ANR-22-CE49-0005-01_ACT) and has benefited from a funding provided by l'Agence Nationale de la Recherche (ANR) under the Generic Call for Proposals 2022.

Funding Open access funding provided by University of Bern.

Declarations

Competing Interests The authors declare that they have no conflict of interest.

References

Abplanalp D, Wurz P, Huber L, Leya I (2010) An optimised compact electron impact ion source for a time-of-flight mass spectrometer. Int J Mass Spectrom 294:33–39. https://doi.org/10.1016/j.ijms.2010.05.001

Arevalo J, Ricardo NZ, Danell RM (2020) Mass spectrometry and planetary exploration: a brief review and future projection. J Mass Spectrom 55:e4454. https://doi.org/10.1002/jms.4388

Ashcroft AE (2007) Ionization methods in organic mass spectrometry. Royal Society of Chemistry, London

Aslam S, Achterberg RK, Calcutt SB, Cottini V, Gorius NJ, Hewagama T, Irwin PG, Nixon CA, Quilligan G, Roos-Serote M, Simon AA, Tran D, Villanueva G (2020) Advanced Net Flux Radiometer for the ice giants. Space Sci Rev 216(1):11. https://doi.org/10.1007/s11214-019-0630-x

Atreya SK, Hofstadter MH, Reh K, In JH, Mousis O, Wong MH (2019) Icy giant planet exploration: are entry probes essential? Acta Astronaut 162:266–274. https://doi.org/10.1016/j.actaastro.2019.06.020. http://www.sciencedirect.com/science/article/pii/S0094576519302668

Bailey E, Stevenson DJ (2021) Thermodynamically governed interior models of Uranus and Neptune. Planet Sci J 2(2):64. https://doi.org/10.3847/PSJ/abd1e0. arXiv:2012.04166

Baines KH, Mickelson ME, Larson LE, Ferguson DW (1995) The abundances of methane and ortho/para hydrogen on Uranus and Neptune: implications of new laboratory 4-0 H_2 quadrupole line parameters. Icarus 114(2):328–340. https://doi.org/10.1006/icar.1995.1065

Balsiger H, Altwegg K, Benson J, Buhler F, Fischer J, Geiss J, Goldstein BE, Goldstein R, Hemmerich P, Kulzer G, Lazarus AJ, Meier A, Neugebauer M, Rettenmund U, Rosenbauer H, Sager K, Sanders T, Schwenn R, Shelley EG, Simpson D, Young DT (1987) The ion mass spectrometer on Giotto. J Phys E, Sci Instrum 20(6):759. https://doi.org/10.1088/0022-3735/20/6/034

Balsiger H, Altwegg K, Arijs E, Bertaux JL, Berthelier JJ, Bochsler P, Carignan G, Eberhardt P, Fisk L, Fuselier S, Ghielmetti A, Gliem F, Gombosi T, Kopp E, Korth A, Livi S, Mazelle C, Rème H, Sauvaud J, Shelley E, Waite J, Wilken B, Woch J, Wollnik H, Wurz P, Young D (1998) Rosetta Orbiter Spectrometer for Ion and Neutral Analysis—ROSINA. Adv Space Res 21(11):1527–1535. https://doi.org/10.1016/S0273-1177(97)00945-9

Balsiger H, Altwegg K, Bochsler P, Eberhardt P, Fischer J, Graf S, Jäckel A, Kopp E, Langer U, Mildner M, Müller J, Riesen T, Rubin M, Scherer S, Wurz P, Wüthrich S, Arijs E, Delanoye S, Keyser JD, Neefs E, Dand Rème NH, Aoustin C, Mazelle C, Médale JL, Sauvaud JA, Berthelier JJ, Bertaux JL, Duvet L, Illiano JM, Fuselier SA, Ghielmetti AG, Magoncelli T, Shelley EG, Korth A, Heerlein K, Lauche H, Livi S, Loose A, Mall U, Wilken B, Gliem F, Fiethe B, Gombosi TI, Block B, Carignan GR, Fisk LA, Waite JH, Young DT, Wollnik H (2007) Rosina – Rosetta Orbiter Spectrometer for Ion and Neutral Analysis. Space Sci Rev 128(1):745–801. https://doi.org/10.1007/s11214-006-8335-3

Banfield D, Schindel DW, Tarr S, Dissly RW (2016) A Martian acoustic anemometer. J Acoust Soc Am 140(2):1420–1428. https://doi.org/10.1121/1.4960737

Barabash S, Wurz P, Brandt P, Wieser M, Holmström M, Futaana Y, Stenberg G, Nilsson H, Eriksson A, Tulej M, Vorburger A, Thomas N, Paranicas C, Mitchell DG, Ho G, Mauk BH, Haggerty D, Westlake JH, Fränz M, Krupp N, Roussos E, Kallio E, Schmidt W, Szego K, Szalai S, Khurana K, Jia X, Paty C, Wimmer-Schweingruber RF, Heber B, Kazushi A, Grande M, Lammer H, Zhang T, McKenna-Lawlor S, Krimigis SM, Sarris T, Grodent D (2013) Particle Environment Package (PEP). In: European Planetary Science Congress, pp EPSC2013–709

Barshick CM, Goodner KL, Watson CH, Eyler JR (1998) Application of glow discharge Fourier-transform ion cyclotron resonance mass spectrometry to isotope ratio measurements11dedicated to the memory of al nier. Int J Mass Spectrom 178(1):73–79. https://doi.org/10.1016/S1387-3806(98)14087-3.

Beckey HD (1970) Field ionisation mass spectrometry. Pergamon Press, Oxford

Benninghoven A, Rüdenauer FG, Werner HW (1987) Secondary ion mass spectrometry—basic concepts, instrumental aspects, applications and trends. Surface and interface analysis. Wiley, New York. https://doi.org/10.1002/sia.740100811

Berthelier JJ, Illiano JM, Nevejans D, Neefs E, Arijs E, Schoon N (2002) High resolution focal plane detector for a space-borne magnetic mass spectrometer. Int J Mass Spectrom 215(1):89–100. https://doi.org/10.1016/S1387-3806(02)00527-4

Bhardwaj A, Mohankumar SV, Das TP, Pradeepkumar P, Sreelatha P, Sundar B, Nandi A, Vajja DP, Dhanya MB, Naik N, Supriya G, Satheesh Thampi R, Padma Padmanabhan G, Yadav VK, Aliyas AV (2016) MENCA experiment aboard India's Mars orbiter mission. Curr Sci 109(6):1106–1113. https://doi.org/10.18520/v109/i6/1106-1113

Bolton SJ, Adriani A, Adumitroaie V, Allison M, Anderson J, Atreya S, Bloxham J, Brown S, Connerney JEP, DeJong E, Folkner W, Gautier D, Grassi D, Gulkis S, Guillot T, Hansen C, Hubbard WB, Iess L, Ingersoll A, Janssen M, Jorgensen J, Kaspi Y, Levin SM, Li C, Lunine J, Miguel Y, Mura A, Orton G, Owen T, Ravine M, Smith E, Steffes P, Stone E, Stevenson D, Thorne R, Waite J, Durante D, Ebert RW, Greathouse TK, Hue V, Parisi M, Szalay JR, Wilson R (2017) Jupiter's interior and deep atmosphere: the initial pole-to-pole passes with the Juno spacecraft. Science 356(6340):821–825. https://doi.org/10.1126/science.aal2108

Brockwell TG, Meech KJ, Pickens K, Waite JH, Miller G, Roberts J, Lunine JI, Wilson P (2016) The mass spectrometer for planetary exploration (MASPEX). In: 2016 IEEE Aerospace Conference, pp 1–17. https://doi.org/10.1109/AERO.2016.7500777

Burgdorf M, Orton GS, Davis GR, Sidher SD, Feuchtgruber H, Griffin MJ, Swinyard BM (2003) Neptune's far-infrared spectrum from the ISO long-wavelength and short-wavelength spectrometers. Icarus 164(1):244–253. https://doi.org/10.1016/S0019-1035(03)00138-6

Cavalié T, Lunine J, Mousis O (2023) A subsolar oxygen abundance or a radiative region deep in Jupiter revealed by thermochemical modelling. Nat Astron 7:678–683. https://doi.org/10.1038/s41550-023-01928-8. arXiv:2305.13949

Chou L, Mahaffy P, Trainer M, Eigenbrode J, Arevalo R, Brinckerhoff W, Getty S, Grefenstette N, Da Poian V, Fricke GM, Kempes CP, Marlow J, Sherwood Lollar B, Graham H, Johnson SS (2021) Planetary mass spectrometry for agnostic life detection in the Solar System. Front Astron Space Sci 8:173. https://doi.org/10.3389/fspas.2021.755100

Cohen IJ, Beddingfield C, Chancia R, DiBraccio G, Hedman M, MacKenzie S, Mauk B, Sayanagi KM, Soderlund KM, Turtle E, Ahrens C, Arridge CS, Brooks SM, Bunce E, Charnoz S, Coustenis A, Dillman RA, Dutta S, Fletcher LN, Harbison R, Helled R, Holme R, Jozwiak L, Kasaba Y, Kollmann P, Luszcz-Cook S, Mandt K, Mousis O, Mura A, Murakami G, Parisi M, Rymer A, Stanley S, Stephan K, Vervack J, Ronald J, Wong MH, Wurz P (2022) The case for a new frontiers-class Uranus orbiter: system science at an underexplored and unique world with a mid-scale mission. Planetary Sci J 3(3):58. https://doi.org/10.3847/PSJ/ac5113

Colin L (1979) Encounter with Venus: an update. Science 205(4401):44–46. https://doi.org/10.1126/science.205.4401.44

Conrath BJ, Gautier D (2000) Saturn helium abundance: a reanalysis of Voyager measurements. Icarus 144(1):124–134. https://doi.org/10.1006/icar.1999.6265

Conrath B, Gautier D, Hanel R, Lindal G, Marten A (1987) The helium abundance of Uranus from Voyager measurements. J Geophys Res 92(A13):15,003–15,010. https://doi.org/10.1029/JA092iA13p15003

Cotter R (1997) Time-of-flight mass spectrometry: instrumentation and applications in biological research (ACS professional reference book). Am. Chem. Soc., Washington

Curtis CC, Fan CY, Hsieh KC, Hunten DM, Ip WH, Keppler E, Richter AK, Umlauft G, Afonin VV, Dyachkov AV, Ero JJ, Somogyi AJ (1987) Comet p/ alley neutral gas density profile along the VEGA-1 trajectory measured by the neutral gas experiment. Astron Astrophys 187:360

Dawson PH (1979) Quadrupole mass spectrometry and its applications. Elsevier, Amsterdam

Eiler J, Cesar J, Chimiak L, Dallas B, Grice K, Griep-Raming J, Juchelka D, Kitchen N, Lloyd M, Makarov A, Robins R, Schwieters J (2017) Analysis of molecular isotopic structures at high precision and accuracy by orbitrap mass spectrometry. Int J Mass Spectrom 422:126–142, https://doi.org/10.1016/j.ijms.2017.10.002

Eriksson LEJ, Mol Lous MAS, Shibata S, Helled R (2023) Can Uranus and Neptune form concurrently via pebble, gas, and planetesimal accretion? Mon Not R Astron Soc 526(4):4860–4876. https://doi.org/10.1093/mnras/stad3007. arXiv:2310.00075

Fausch RG, Wurz P, Tulej M, Jost J, Gubler P, Gruber M, Lasi D, Zimmermann C, Gerber T (2018) Flight electronics of gc-mass spectrometer for investigation of volatiles in the lunar regolith. In: 2018 IEEE Aerospace Conference, pp 1–13. https://doi.org/10.1109/AERO.2018.8396788

Ferri F, Angrilli F, Bianchini G, Fulchignoni M (HASI Team) (2002) Huygens atmospheric structure instrument of Huygens probe on Cassini mission. Acta Astronaut 50(4):249–255. https://doi.org/10.1016/S0094-5765(01)00161-8

Ferri F, Colombatti G, Aboudan A, Bettanini C, Debei S, Harri AM, Lebreton JP, Montmessin F, Berthelier JJ, LeGall A, Modolo R, Aplin K, Coustenis A (2020) The atmospheric structure of the ice giant planets from in situ measurements by entry probes. Space Sci Rev 216(8):118. https://doi.org/10.1007/s11214-020-00749-9

Feuchtgruber H, Lellouch E, Orton G, de Graauw T, Vandenbussche B, Swinyard B, Moreno R, Jarchow C, Billebaud F, Cavalié T, Sidher S, Hartogh P (2013) The D/H ratio in the atmospheres of Uranus and Neptune from Herschel-PACS observations. Astron Astrophys 551:A126. https://doi.org/10.1051/0004-6361/201220857. arXiv:1301.5781

Fletcher LN, Orton GS, Teanby NA, Irwin PGJ (2009a) Phosphine on Jupiter and Saturn from Cassini/CIRS. Icarus 202(2):543–564. https://doi.org/10.1016/j.icarus.2009.03.023

Fletcher LN, Orton GS, Teanby NA, Irwin PGJ, Bjoraker GL (2009b) Methane and its isotopologues on Saturn from Cassini/CIRS observations. Icarus 199(2):351–367. https://doi.org/10.1016/j.icarus.2008.09.019

Fletcher LN, Baines KH, Momary TW, Showman AP, Irwin PGJ, Orton GS, Roos-Serote M, Merlet C (2011) Saturn's tropospheric composition and clouds from Cassini/VIMS 4.6-5.1 μm nightside spectroscopy. Icarus 214(2):510–533. https://doi.org/10.1016/j.icarus.2011.06.006

Fletcher LN, Greathouse TK, Orton GS, Irwin PGJ, Mousis O, Sinclair JA, Giles RS (2014) The origin of nitrogen on Jupiter and Saturn from the 15N/14N ratio. Icarus 238:170

Fletcher LN, Helled R, Roussos E, Jones G, Charnoz S, André N, Andrews D, Bannister M, Bunce E, Cavalié T, Ferri F, Fortney J, Grassi D, Griton L, Hartogh P, Hueso R, Kaspi Y, Lamy L, Masters A, Melin H, Moses J, Mousis O, Nettleman N, Plainaki C, Schmidt J, Simon A, Tobie G, Tortora P, Tosi F, Turrini D (2022) Ice giant system exploration within ESA's Voyage 2050. Exp Astron 54(2–3):1015–1025. https://doi.org/10.1007/s10686-021-09759-z

Föhn M, Galli A, Vorburger A, Tulej M, Lasi D, Riedo A, Fausch RG, Althaus M, Brüngger S, Fahrer P, Gerber M, Lüthi M, Munz HP, Oeschger S, Piazza D, Wurz P (2021) Description of the mass spectrometer for the Jupiter Icy moons Explorer mission. In: 2021 IEEE Aerospace Conference 50100:1–14. https://doi.org/10.1109/AERO50100.2021.9438344

Fortney JJ, Hubbard WB (2004) Effects of helium phase separation on the evolution of extrasolar giant planets. Astrophys J 608(2):1039–1049. https://doi.org/10.1086/420765. arXiv:astro-ph/0402620

Fulchignoni M, Angrilli F, Bianchini G, Bar-Nun A, Barucci MA, Borucki W, Coradini M, Coustenis A, Ferri F, Grard RJ, Hemelin M, Harri AM, Leppelmeier GW, Lopez-Moreno JJ, McDonnell JAM, McKay C, Neubauer FM, Pedersen A, Picardi G, Pirronello V, Pirjola R, Rodrigo R, Schwingenschuh C, Seiff A, Svedhem H, Vanzani V, Visconti G, Zarnecki J, Thrane E (1997) The Huygens atmospheric structure instrument. In: Wilson A (ed) Huygens: science, payload and mission, ESA Special Publication. vol 1177 p 163

Fulchignoni M, Ferri F, Angrilli F, Bar-Nun A, Barucci MA, Bianchini G, Borucki W, Coradini M, Coustenis A, Falkner P, Flamini E, Grard R, Hamelin M, Harri AM, Leppelmeier GW, Lopez-Moreno JJ, McDonnell JAM, McKay CP, Neubauer FH, Pedersen A, Picardi G, Pirronello V, Rodrigo R, Schwingenschuh K, Seiff A, Svedhem H, Vanzani V, Zarnecki J (2002) The characterisation of Titan's atmospheric physical properties by the Huygens Atmospheric Structure Instrument (HASI). Space Sci Rev 104(1):395–431. https://doi.org/10.1023/A:1023688607077

Gautier D, Hersant F, Mousis O, Lunine JI (2001) Enrichments in volatiles in Jupiter: a new interpretation of the Galileo measurements. Astrophys J Lett 550(2):L227–L230. https://doi.org/10.1086/319648

Gierasch PJ, Conrath BJ (1987) Vertical temperature gradients on Uranus: implications for layered convection. J Geophys Res 92(A13):15,019–15,029. https://doi.org/10.1029/JA092iA13p15019

Glassmeier KH, Boehnhardt H, Koschny D, Kührt E, Richter I (2007) The Rosetta mission: flying towards the origin of the Solar System. Space Sci Rev 128(1–4):1–21. https://doi.org/10.1007/s11214-006-9140-8

Goesmann F, Rosenbauer H, Roll R, Szopa C, Raulin F, Sternberg R, Israel G, Meierhenrich U, Thiemann W, Munoz-Caro G (2007) Cosac, the cometary sampling and composition experiment on Philae. Space Sci Rev 128(1–4):257–280. https://doi.org/10.1007/s11214-006-9000-6

Goesmann F, Rosenbauer H, Bredehöft JH, Cabane M, Ehrenfreund P, Gautier T, Giri C, Krüger H, Le Roy L, MacDermott AJ, McKenna-Lawlor S, Meierhenrich UJ, Caro GMM, Raulin F, Roll R, Steele A, Steininger H, Sternberg R, Szopa C, Thiemann W, Ulamec S (2015) Organic compounds on comet 67P/Churyumov-Gerasimenko revealed by COSAC mass spectrometry. Science 349(6247):2.689. https://doi.org/10.1126/science.aab0689

Goesmann F, Brinckerhoff WB, Raulin F, Goetz W, Danell RM, Getty SA, Siljeström S, Mißbach H, Steininger H, Arevalo J, Ricardo D, Buch A, Freissinet C, Grubisic A, Meierhenrich UJ, Pinnick VT, Stalport F, Szopa C, Vago JL, Lindner R, Schulte MD, Brucato JR, Glavin DP, Grand N, Li X (van Amerom FHW, MOMA Science Team) (2017) The Mars Organic Molecule Analyzer (MOMA) instrument: characterization of organic material in Martian sediments. Astrobiology 17(6–7):655–685. https://doi.org/10.1089/ast.2016.1551

Grinfeld D, Stewart H, Skoblin M, Denisov E, Monastryrsky M, Makarov A (2019) Space-charge dynamics in Orbitrap mass spectrometers. Int J Mod Phys A 34(36):1942007. https://doi.org/10.1142/S0217751X19420077

Guillot T, Hueso R (2006) The composition of Jupiter: sign of a (relatively) late formation in a chemically evolved protosolar disc. Mon Not R Astron Soc 367(1):L47–L51. https://doi.org/10.1111/j.1745-3933.2006.00137.x. arXiv:astro-ph/0601043

Guillot T, Fortney J, Rauscher E, Marley MS, Parmentier V, Line M, Wakeford H, Kaspi Y, Helled R, Ikoma M, Knutson H, Menou K, Valencia D, Durante D, Ida S, Bolton SJ, Li C, Stevenson KB, Bean J, Cowan NB, Hofstadter MD, Hueso R, Leconte J, Li L, Mordasini C, Mousis O, Nettelmann N, Soderlund K, Wong MH (2020) Keys of a Mission to Uranus or Neptune, the Closest Ice Giants. https://doi.org/10.48550/arXiv.2012.09863. arXiv:2012.09863

Gurnee RS, Livi S, Phillips ML, Desai MI, Hayes JR, Ho GC, Hourani R, Jaskulek S, Scheer J (2012) Strofio: a novel neutral mass spectrograph for sampling Mercury's exosphere. In: 2012 IEEE Aerospace Conference, pp 1–11. https://doi.org/10.1109/AERO.2012.6187066

Harrison AG (2017) Chemical ionization mass spectrometry. Routledge, Taylor & Francis Group. https://doi.org/10.1201/9781315139128

Helled R (2023) The mass of gas giant planets: is Saturn a failed gas giant? Astron Astrophys 675:L8. https://doi.org/10.1051/0004-6361/202346850. arXiv:2306.14740

Helled R, Bodenheimer P (2014) The formation of Uranus and Neptune: challenges and implications for intermediate-mass exoplanets. Astrophys J 789(1):69. https://doi.org/10.1088/0004-637X/789/1/69. arXiv:1404.5018

Helled R, Fortney JJ (2020) The interiors of Uranus and Neptune: current understanding and open questions. Philos Trans R Soc Lond Ser A 378(2187):20190474. https://doi.org/10.1098/rsta.2019.0474. arXiv:2007.10783

Helled R, Nettelmann N, Guillot T (2020) Uranus and Neptune: origin, evolution and internal structure. Space Sci Rev 216(3):38. https://doi.org/10.1007/s11214-020-00660-3. arXiv:1909.04891

Hoegg ED, Barinaga CJ, Hager GJ, Hart GL, Koppenaal DW, Marcus RK (2016) Preliminary figures of merit for isotope ratio measurements: the liquid sampling-atmospheric pressure glow discharge microplasma ionization source coupled to an orbitrap mass analyzer. J Am Soc Mass Spectrom 27(8):1393–1403. https://doi.org/10.1007/s13361-016-1402-4

Hoegg ED, Barinaga CJ, Hager GJ, Hart GL, Koppenaal DW, Marcus RK (2016b) Isotope ratio characteristics and sensitivity for uranium determinations using a liquid sampling-atmospheric pressure glow discharge ion source coupled to an orbitrap mass analyzer. J Anal At Spectrom 31:2355–2362. https://doi.org/10.1039/C6JA00163G

Hofer L, Wurz P, Buch A, Cabane M, Coll P, Coscia D, Gerasimov M, Lasi D, Sapgir A, Szopa C, Tulej M (2015) Prototype of the gas chromatograph - mass spectrometer to investigate volatile species in the lunar soil for the Luna-resurs mission. Planet Space Sci 111:126–133

Hoffman JH, Hodges JRR, Evans DE (1972) Lunar orbital mass spectrometer experiment. In: Lunar and Planetary Science Conference proceedings, vol 3, p 2205

Hoffman JH, Hodges JRR, Evans DE (1973) Lunar atmospheric composition results from Apollo 17. In: Lunar and Planetary Science Conference, Lunar and Planetary Science Conference, vol 4, p 376

Hoffman J, Chaney R, Hammack H (2008) Phoenix Mars mission—the thermal evolved gas analyze. J Am Soc Mass Spectrom 19:1377–1383. https://doi.org/10.1016/j.jasms.2008.07.015

Hu Q, Noll RJ, Li H, Makarov A, Hardman M, Graham Cooks R (2005) The orbitrap: a new mass spectrometer. J Mass Spectrom 40(4):430–443. https://doi.org/10.1002/jms.856

Hueso R, Sánchez-Lavega A (2019) Atmospheric dynamics and vertical structure of Uranus and Neptune's weather layers. Space Sci Rev 215(8):52. https://doi.org/10.1007/s11214-019-0618-6

Hughes RJ, March R, Todd JFJ (2005) Quadrupole ion trap mass spectrometry. Wiley, New York

Irwin PGJ, Toledo D, Garland R, Teanby NA, Fletcher LN, Orton GA, Bézard B (2018) Detection of hydrogen sulfide above the clouds in Uranus's atmosphere. Nat Astron 2:420–427. https://doi.org/10.1038/s41550-018-0432-1

Irwin PGJ, Toledo D, Garland R, Teanby NA, Fletcher LN, Orton GS, Bézard B (2019) Probable detection of hydrogen sulphide (H_2S) in Neptune's atmosphere. Icarus 321:550–563. https://doi.org/10.1016/j.icarus.2018.12.014. arXiv:1812.05382

Istomin V (1982) Venera mass spectrometer data on atmospheric composition. USSR Rep Space 17:30–33

Istomin V, Grechnev K, Kotchnev V (1980) Mass spectrometer measurements of the composition of the lower atmosphere of Venus. In: Rycroft M (ed) Space research. COSPAR colloquia series, vol 20. Pergamon, Elmsford, pp 215–218. https://doi.org/10.1016/S0964-2749(13)60044-X

Karkoschka E, Tomasko M (2009) The haze and methane distributions on Uranus from HST-STIS spectroscopy. Icarus 202(1):287–309. https://doi.org/10.1016/j.icarus.2009.02.010

Karkoschka E, Tomasko MG (2011) The haze and methane distributions on Neptune from HST-STIS spectroscopy. Icarus 211(1):780–797. https://doi.org/10.1016/j.icarus.2010.08.013

Kaspi Y, Showman AP, Hubbard WB, Aharonson O, Helled R (2013) Atmospheric confinement of jet streams on Uranus and Neptune. Nature 497(7449):344–347. https://doi.org/10.1038/nature12131

Krankowsky D, Lammerzahl P, Herrwerth I, Woweries J, Eberhardt P, Dolder U, Herrmann U, Schulte W, Berthelier JJ, Illiano JM, Hodges RR, Hoffman JH (1986) In situ gas and ion measurements at comet Halley. Nature 321:326–329. https://doi.org/10.1038/321326a0

Kurosaki K, Ikoma M (2017) Acceleration of cooling of ice giants by condensation in early atmospheres. Astron J 153(6):260. https://doi.org/10.3847/1538-3881/aa6faf. arXiv:1704.07558

Le Roy L, Altwegg K, Balsiger H, Berthelier JJ, Bieler A, Briois C, Calmonte U, Combi MR, De Keyser J, Dhooghe F, Fiethe B, Fuselier SA, Gasc S, Gombosi TI, Hässig M, Jäckel A, Rubin M, Tzou CY (2015) Inventory of the volatiles on comet 67P/Churyumov-Gerasimenko from Rosetta/ROSINA. Astron Astrophys 583:A1. https://doi.org/10.1051/0004-6361/201526450

Lellouch E, Bézard B, Fouchet T, Feuchtgruber H, Encrenaz T, de Graauw T (2001) The deuterium abundance in Jupiter and Saturn from ISO-SWS observations. Astron Astrophys 370:610–622. https://doi.org/10.1051/0004-6361:20010259

Li C, Ingersoll A, Bolton S, Levin S, Janssen M, Atreya S, Lunine J, Steffes P, Brown S, Guillot T, Allison M, Arballo J, Bellotti A, Adumitroaie V, Gulkis S, Hodges A, Li L, Misra S, Orton G, Oyafuso F, Santos-Costa D, Waite H, Zhang Z (2020) The water abundance in Jupiter's equatorial zone. Nat Astron 4:609–616. https://doi.org/10.1038/s41550-020-1009-3. arXiv:2012.10305

Lindal GF, Lyons JR, Sweetnam DN, Eshleman VR, Hinson DP, Tyler GL (1987) The atmosphere of Uranus: results of radio occultation measurements with Voyager 2. J Geophys Res 92(A13):14,987–15,001. https://doi.org/10.1029/JA092iA13p14987

Lindal GF, Lyons JR, Sweetnam DN, Eshleman VR, Hinson DP, Tyler GL (1990) The atmosphere of Neptune: results of radio occultation measurements with the Voyager 2 spacecraft. Geophys Res Lett 17(10):1733–1736. https://doi.org/10.1029/GL017i010p01733

Mahaffy PR, Donahue TM, Atreya SK, Owen TC, Niemann HB (1998) Galileo Probe measurements of D/H and 3He/4He in Jupiter's atmosphere. Space Sci Rev 84:251–263

Mahaffy PR, Niemann HB, Alpert A, Atreya SK, Demick J, Donahue TM, Harpold DN, Owen TC (2000) Noble gas abundance and isotope ratios in the atmosphere of Jupiter from the Galileo Probe Mass Spectrometer. J Geophys Res 105(E6):15,061–15,072. https://doi.org/10.1029/1999JE001224

Mahaffy PR, Webster CR, Cabane M, Conrad PG, Coll P, Atreya SK, Arvey R, Barciniak M, Benna M, Bleacher L, Brinckerhoff WB, Eigenbrode JL, Carignan D, Cascia M, Chalmers RA, Dworkin JP, Errigo T, Everson P, Franz H, Farley R, Feng S, Frazier G, Freissinet A, Glavin DP, Harpold DN, Hawk D, Holmes V, Johnson CS, Jones A, Jordan P, Kellogg J, Lewis J, Lyness E, Malespin CA, Martin DK, Maurer J, McAdam AC, McLennan D, Nolan TJ, Noriega M, Pavlov AA, Prats B, Raaen E, Sheinman O, Sheppard D, Smith J, Stern JC, Tan F, Trainer M, Ming DW, Morris RV, Jones J, Gundersen C, Steele A, Wray J, Botta O, Leshin LA, Owen T, Battel S, Jakosky BM, Manning H, Squyres S, Navarro-González R, McKay CP, Raulin F, Sternberg R, Buch A, Sorensen P, Kline-Schoder R, Coscia D, Szopa C, Teinturier S, Baffes C, Feldman J, Flesch G, Forouhar S, Garcia R, Keymeulen D, Woodward S, Block BP, Arnett K, Miller R, Edmonson C, Gorevan S, Mumm E (2012) The sample analysis at Mars investigation and instrument suite. Space Sci Rev 170(1):401–478. https://doi.org/10.1007/s11214-012-9879-z

Mahaffy PR, Richard Hodges R, Benna M, King T, Arvey R, Barciniak M, Bendt M, Carigan D, Errigo T, Harpold DN, Holmes V, Johnson CS, Kellogg J, Kimvilakani P, Lefavor M, Hengemihle J, Jaeger F, Lyness E, Maurer J, Nguyen D, Nolan TJ, Noreiga F, Noriega M, Patel K, Prats B, Quinones O, Raaen E, Tan F, Weidner E, Woronowicz M, Gundersen C, Battel S, Block BP, Arnett K, Miller R, Cooper C, Edmonson C (2014) The Neutral Mass Spectrometer on the lunar atmosphere and Dust Environment Explorer Mission. Space Sci Rev 185(1–4):27–61. https://doi.org/10.1007/s11214-014-0043-9

Mahaffy PR, Benna M, King T, Harpold DN, Arvey R, Barciniak M, Bendt M, Carrigan D, Errigo T, Holmes V, Johnson CS, Kellogg J, Kimvilakani P, Lefavor M, Hengemihle J, Jaeger F, Lyness E, Maurer J, Melak A, Noreiga F, Noriega M, Patel K, Prats B, Raaen E, Tan F, Weidner E, Gundersen C, Battel S, Block BP, Arnett K, Miller R, Cooper C, Edmonson C, Nolan JT (2015) The neutral gas and ion mass spectrometer on the Mars atmosphere and Volatile Evolution Mission. Space Sci Rev 195(1–4):49–73. https://doi.org/10.1007/s11214-014-0091-1

Makarov A, Denisov E, Lange O (2009) Performance evaluation of a high-field orbitrap mass analyzer. J Am Soc Mass Spectrom 20:1391–1396. https://doi.org/10.1016/j.jasms.2009.01.005

Mandt KE, Mousis O, Lunine J, Marty B, Smith T, Luspay-Kuti A, Aguichine A (2020) Tracing the origins of the ice giants through noble gas isotopic composition. Space Sci Rev 216(5):99. https://doi.org/10.1007/s11214-020-00723-5

Marty B, Altwegg K, Balsiger H, Bar-Nun A, Bekaert DV, Berthelier JJ, Bieler A, Briois C, Calmonte U, Combi M, De Keyser J, Fiethe B, Fuselier SA, Gasc S, Gombosi TI, Hansen KC, Hässig M, Jäckel A, Kopp E, Korth A, Le Roy L, Mall U, Mousis O, Owen T, Rème H, Rubin M, Sémon T, Tzou CY, Waite JH, Wurz P (2017) Xenon isotopes in 67P/Churyumov-Gerasimenko show that comets contributed to Earth's atmosphere. Science 356(6342):1069–1072. https://doi.org/10.1126/science.aal3496

McLafferty FW, Turecek F (1993) Interpretation of mass spectra. University Science Books

Meyer S, Tulej M, Wurz P (2017) Mass spectrometry of planetary exospheres at high relative velocity: direct comparison of open- and closed-source measurements. Geosci Instrum Method Data Syst 6(1):1–8. https://doi.org/10.5194/gi-6-1-2017

Miller K, Miller G, Waite H, Brockwell T, Franke K, Hoeper P, Perryman R, Glein C, Burch J (2022) Onwards to Europa: results from the final ground calibration of the MASPEX-Europa flight instrument. In: European Planetary Science Congress, p EPSC2022–705. https://doi.org/10.5194/epsc2022-705

Molter EM, de Pater I, Luszcz-Cook S, Tollefson J, Sault RJ, Butler B, de Boer D (2021) Tropospheric composition and circulation of Uranus with ALMA and the VLA. Planetary Sci J 2(1):3. https://doi.org/10.3847/PSJ/abc48a

Moses JI, Fletcher LN, Greathouse TK, Orton GS, Hue V (2018) Seasonal stratospheric photochemistry on Uranus and Neptunes. Icarus 307:124–145. https://doi.org/10.1016/j.icarus.2018.02.004

Mousis O, Marboeuf U, Lunine JI, Alibert Y, Fletcher LN, Orton GS, Pauzat F, Ellinger Y (2009) Determination of the minimum masses of heavy elements in the envelopes of Jupiter and Saturn. Astrophys J 696(2):1348–1354. https://doi.org/10.1088/0004-637X/696/2/1348. arXiv:0812.2441

Mousis O, Fletcher LN, Lebreton JP, Wurz P, Cavalié T, Coustenis A, Courtin R, Gautier D, Helled R, Irwin PGJ, Morse AD, Nettelmann N, Marty B, Rousselot P, Venot O, Atkinson DH, Waite JH, Reh KR, Simon AA, Atreya S, André N, Blanc M, Daglis IA, Fischer G, Geppert WD, Guillot T, Hedman MM, Hueso R, Lellouch E, Lunine JI, Murray CD, O'Donoghue J, Rengel M, Sánchez-Lavega A, Schmider FX, Spiga A, Spilker T, Petit JM, Tiscareno MS, Ali-Dib M, Altwegg K, Bolton SJ, Bouquet A, Briois C, Fouchet T, Guerlet S, Kostiuk T, Lebleu D, Moreno R, Orton GS, Poncy J (2014) Scientific rationale for Saturn's in situ exploration. Planet Space Sci 104:29–47. https://doi.org/10.1016/j.pss.2014.09.014. arXiv:1404.4811

Mousis O, Atkinson DH, Spilker T, Venkatapathy E, Poncy J, Frampton R, Coustenis A, Reh K, Lebreton JP, Fletcher LN, Hueso R, Amato MJ, Colaprete A, Ferri F, Stam D, Wurz P, Atreya S, Aslam S, Banfield DJ, Calcutt S, Fischer G, Holland A, Keller C, Kessler E, Leese M, Levacher P, Morse A, Muñoz O, Renard JB, Sheridan S, Schmider FX, Snik F, Waite JH, Bird M, Cavalié T, Deleuil M, Fortney J, Gautier D, Guillot T, Lunine JI, Marty B, Nixon C, Orton GS, Sánchez-Lavega A (2016) The Hera Saturn Entry Probe Mission. Planet Space Sci 130:80–103. https://doi.org/10.1016/j.pss.2015.06.020. arXiv:1510.07685

Mousis O, Atkinson DH, Cavalié T, Fletcher LN, Amato MJ, Aslam S, Ferri F, Renard JB, Spilker T, Venkatapathy E, Wurz P, Aplin K, Coustenis A, Deleuil M, Dobrijevic M, Fouchet T, Guillot T, Hartogh P, Hewagama T, Hofstadter MD, Hue V, Hueso R, Lebreton JP, Lellouch E, Moses J, Orton GS, Pearl JC, Sánchez-Lavega A, Simon A, Venot O, Waite JH, Achterberg RK, Atreya S, Billebaud F, Blanc M, Borget F, Brugger B, Charnoz S, Chiavassa T, Cottini V, d'Hendecourt L, Danger G, Encrenaz T, Gorius NJP, Jorda L, Marty B, Moreno R, Morse A, Nixon C, Reh K, Ronnet T, Schmider FX, Sheridan S, Sotin C, Vernazza P, Villanueva GL (2018) Scientific rationale for Uranus and Neptune in situ explorations. Planet Space Sci 155:12–40. https://doi.org/10.1016/j.pss.2017.10.005. arXiv:1708.00235

Mousis O, Aguichine A, Atkinson DH, Atreya SK, Cavalié T, Lunine JI, Mandt KE, Ronnet T (2020) Key atmospheric signatures for identifying the source reservoirs of volatiles in Uranus and Neptune. Space Sci Rev 216(5):77. https://doi.org/10.1007/s11214-020-00681-y. arXiv:2004.11061

Mousis O, Atkinson DH, Ambrosi R, Atreya S, Banfield D, Barabash S, Blanc M, Cavalié T, Coustenis A, Deleuil M, Durry G, Ferri F, Fletcher L, Fouchet T, Guillot T, Hartogh P, Hueso R, Hofstadter M, Lebreton JP, Mandt KE, Rauer H, Rannou P, Renard JB, Sanchez-Lávega A, Sayanagi K, Simon A, Spilker T, Venkatapathy E, Waite JH, Wurz P (2022) In situ exploration of the giant planets. Exp Astron 54:975–1013. https://doi.org/10.1007/s10686-021-09775-z

Mousis O, Ambrosi R, André N, Andrews J, Apéstigue Palacio V, Atkinson D, Arruego Rodriguez I, Blanc M, Boithias H, Bolton S, Bousquet P, Canup R, Cavalié T, Freeman A, Faye F, Ferri F, Glein C, Guelhan A, Hartogh P, Loehle S, Hue V, Lebreton JP, Lemaistre S, Mooij E, Pichon T, Pinaud G, Steuer D, Toledo Carrasco D, Rauer H, Vorburger A, Wurz P (2024) Generic Entry Probe Program (GEPP) – an international initiative promoting the development of European descent modules dedicated to the in situ exploration of giant planets. In: EGU General Assembly 2024, Vienna, Austria, 14-19 Apr 2024, EGU24-13379. https://doi.org/10.5194/egusphere-egu24-13379

National Academies of Sciences, Engineering, and Medicine (2023) Origins, worlds, and life: a decadal strategy for planetary science and astrobiology 2023-2032. Natl. Acad. Press, Washington. https://doi.org/10.17226/26522

Neuenschwander BA, Müller S, Helled R (2024) Uranus' Complex Internal Structure. https://doi.org/10.48550/arXiv.2401.11769. arXiv:2401.11769

Niemann H, Booth J, Cooley J, Hartle R, Kasprzak W, Spencer N, Way S, Hunten D, Carignan G (1980) Pioneer Venus orbiter neutral gas mass spectrometer experiment. IEEE Trans Geosci Remote Sens GE-18:60–65

Niemann HB, Harpold DN, Atreya SK, Carignan GR, Hunten DM, Owen TC (1992) Galileo Probe Mass Spectrometer experiment. Space Sci Rev 60(1-4):111–142. https://doi.org/10.1007/BF00216852

Niemann HB, Atreya SK, Carignan GR, Donahue TM, Haberman JA, Harpold DN, Hartle RE, Hunten DM, Kasprzak WT, Mahaffy PR, Owen TC, Way SH (1998) The composition of the Jovian atmosphere as determined by the Galileo Probe Mass Spectrometer. J Geophys Res 103(E10):22,831–22,846. https://doi.org/10.1029/98JE01050

Niemann HB, Atreya SK, Bauer SJ, Biemann K, Block B, Carignan GR, Donahue TM, Frost RL, Gautier D, Haberman JA, Harpold D, Hunten DM, Israel G, Lunine JI, Mauersberger K, Owen TC, Raulin F, Richards JE, Way SH (2002) The Gas Chromatograph Mass Spectrometer for the Huygens probe. Space Sci Rev 104(1):553–591. https://doi.org/10.1023/A:1023680305259

Niemann HB, Atreya SK, Bauer SJ, Carignan GR, Demick JE, Frost RL, Gautier D, Haberman JA, Harpold DN, Hunten DM, Israel G, Lunine JI, Kasprzak WT, Owen TC, Paulkovich M, Raulin F, Raaen E, Way SH (2005) The abundances of constituents of Titan's atmosphere from the GCMS instrument on the Huygens probe. Nature 438(7069):779–784. https://doi.org/10.1038/nature04122

Niemann HB, Atreya SK, Demick JE, Gautier D, Haberman JA, Harpold DN, Kasprzak WT, Lunine JI, Owen TC, Raulin F (2010) Composition of Titan's lower atmosphere and simple surface volatiles as measured by the Cassini-Huygens probe Gas Chromatograph Mass Spectrometer experiment. J Geophys Res, Planets 115(E12)

Nier AO, McElroy MB (1977) Composition and structure of Mars' upper atmosphere: results from the neutral mass spectrometers on Viking 1 and 2. J Geophys Res 82(28):4341–4349. https://doi.org/10.1029/JS082i028p04341

Nier AO, Hoffman JH, Johnson CY, Holmes JC (1964) Neutral constituents of the upper atmosphere: the minor peaks observed in a mass spectrometer. J Geophys Res 69(21):4629–4636. https://doi.org/10.1029/JZ069i021p04629

Orsini S, Livi S, Torkar K, Barabash S, Milillo A, Wurz P, di Lellis AM, Kallio E (SERENA Team) (2010) SERENA: a suite of four instruments (ELENA, STROFIO, PICAM and MIPA) on board BepiColombo-MPO for particle detection in the Hermean environment. Planet Space Sci 58(1-2):166–181. https://doi.org/10.1016/j.pss.2008.09.012

Orsini S, Livi S, Lichtenegger H, Barabash S, Milillo A, De Angelis E, Phillips M, Laky G, Wieser M, Olivieri A, Plainaki C, Ho G, Killen R, Slavin J, Wurz P, Berthelier JJ, Dandouras I, Dosa M, Kallio E, McKenna-Lawlor S, Torkar K, Vaisberg O, Allegrini F, Daglis I, Dong C, Escoubet C, Fatemi MSF, Ivanovski S, Krupp N, Lammer H, Leblanc F, Mangano V, Mura A, Nilsson H, Raines J, Rispoli R, Sarantos M, Smith H, Szego K, Varsani A, Aronica A, Camozzi F, Di Lellis A, Fremuth G, Giner F, Gurnee R, Hayes J, Jeszenszky H, Tominetti F, Trantham B, Balaz J, Baumjohann W, Brienza D, Bührke U, Bush MD, Cantatore M, Cibella S, Colasanti L, Cremonese G, Cremonesi L, D'Alessandro M, Delcourt D, Delva M, Desai M, Fam'a M, Ferris M, Fischer H, Gaggero A, Gamborino D, Garnier P, Gibson B, Goldstein R, Grande M, Grishin V, Haggerty D, Holmström M, Horvath I, Hsieh K, Jacques A, Johnson R, Kazakov A, Kecskemety K, Krüger H, Kürbisch C, Lazzarotto F, Leblanc F, Leichtfried M, Leoni R, Loose A, Maschietti D, Massetti S, Mattioli F, Miller G, Moissenko D, Morbidini A, Noschese R, Nuccilli F, Nunez C, Paschalidis N, Persyn S, Piazza D, Oja M, Ryno J, Schmidt W, Scheer J, Shestakov A, Shuvalov S, Seki K, Selci S, Smith K, Sordini R, Stenbeck F, Svensson J, Szalai L, Szego K, Toublanc D, Urdiales C, Vertolli N, Wallner R, Wahlstroem P, Wilson P, Zampieri S (2021) Particle instrument suite for determining the Sun-Mercury interaction from BepiColombo. Space Sci Rev 217(11):107. https://doi.org/10.1007/s11214-020-00787-3

Owen T, Mahaffy P, Niemann HB, Atreya S, Donahue T, Bar-Nun A, de Pater I (1999) A low-temperature origin for the planetesimals that formed Jupiter. Nature 402(6759):269–270. https://doi.org/10.1038/46232

Owen T, Mahaffy PR, Niemann HB, Atreya S, Wong M (2001) Protosolar nitrogen. Astrophys J Lett 553(1):L77–L79. https://doi.org/10.1086/320501

Pearl JC, Conrath BJ (1991) The albedo, effective temperature, and energy balance of Neptune, as determined from Voyager data. J Geophys Res 96:18,921–18,930. https://doi.org/10.1029/91JA01087

Pearl JC, Conrath BJ, Hanel RA, Pirraglia JA, Coustenis A (1990) The albedo, effective temperature, and energy balance of Uranus, as determined from Voyager IRIS data. Icarus 84(1):12–28. https://doi.org/10.1016/0019-1035(90)90155-3

Rubin M, Altwegg K, Balsiger H, Berthelier JJ, Combi MR, De Keyser J, Drozdovskaya M, Fiethe B, Fuselier SA, Gasc S, Gombosi TI, Hänni N, Hansen KC, Mall U, Rème H, Schroeder IRHG, Schuhmann M, Sémon T, Waite JH, Wampfler SF, Wurz P (2019a) Elemental and molecular abundances in comet 67P/Churyumov-Gerasimenko. Mon Not R Astron Soc 489(1):594–607. https://doi.org/10.1093/mnras/stz2086. arXiv:1907.11044

Rubin M, Bekaert DV, Broadley MW, Drozdovskaya MN, Wampfler SF (2019b) Volatile species in comet 67P/Churyumov-Gerasimenko: investigating the link from the ISM to the terrestrial planets. ACS Earth and Space Chemistry 3(9):1792–1811. https://doi.org/10.1021/acsearthspacechem.9b00096. arXiv:1908.02960

Rushneck DR, Diaz AV, Howarth DW, Rampacek J, Olson KW, Dencker WD, Smith P, McDavid L, Tomassian A, Harris M, Bulota K, Biemann K, LaFleur AL, Biller JE, Owen T (1978) Viking gas chromatograph-mass spectrometer. Rev Sci Instrum 49(6):817–834. https://doi.org/10.1063/1.1135623

Scherer S, Altwegg K, Balsiger H, Fischer J, Jäckel A, Korth A, Mildner M, Piazza D, Reme H, Wurz P (2006) A novel principle for an ion mirror design in time-of-flight mass spectrometry. Int J Mass Spectrom 251(1):73–81. https://doi.org/10.1016/j.ijms.2006.01.025

Soyuer D, Helled R (2021) Linking Uranus' temperature profile to wind-induced magnetic fields. Mon Not R Astron Soc 507(1):1485–1490. https://doi.org/10.1093/mnras/stab2274. arXiv:2108.01604

Soyuer D, Soubiran F, Helled R (2020) Constraining the depth of the winds on Uranus and Neptune via ohmic dissipation. Mon Not Roy Acad Sci 498:621–638. https://doi.org/10.1093/mnras/staa2461

Soyuer D, Neuenschwander B, Helled R (2023) Zonal winds of Uranus and Neptune: gravitational harmonics, dynamic self-gravity, shape, and rotation. Astron J 165(1):27. https://doi.org/10.3847/1538-3881/aca08d. arXiv:2210.17389

Spell TL, DeLong SE, Creasy WR (1993) Characterization of Fourier transform ion cyclotron resonance mass spectrometry for quantitative isotope ratio measurements. Int J Mass Spectrom Ion Process 124(3):223–239. https://doi.org/10.1016/0168-1176(93)80093-T

Sridharan R, Ahmed SM, Pratim Das T, Sreelatha P, Pradeepkumar P, Naik N, Supriya G (2010) 'Direct' evidence for water (H_2O) in the sunlit lunar ambience from Chace on MIP of Chandrayaan I. Planet Space Sci 58(6):947–950. https://doi.org/10.1016/j.pss.2010.02.013

Sromovsky LA, Karkoschka E, Fry PM, Hammel HB, de Pater I, Rages K (2014) Methane depletion in both polar regions of Uranus inferred from HST/STIS and Keck/NIRC2 observations. Icarus 238:137

Sromovsky LA, de Pater I, Fry PM, Hammel HB, Marcus P (2015) High S/N Keck and Gemini AO imaging of Uranus during 2012-2014: new cloud patterns, increasing activity, and improved wind measurements. Icarus 258:192–223. https://doi.org/10.1016/j.icarus.2015.05.029. arXiv:1512.05009

Stevenson DJ, Salpeter EE (1977) The phase diagram and transport properties for hydrogen-helium fluid planets. Astrophys J Suppl Ser 35:221–237. https://doi.org/10.1086/190478

Taylor HA, Brinton HC, Wagner TCG, Blackwell BH, Cordier GR (1980) Bennett ion mass spectrometers on the pioneer Venus bus and orbiter. IEEE Trans Geosci Remote Sens GE-18(1):44–49. https://doi.org/10.1109/TGRS.1980.350259

Valletta C, Helled R (2022) Possible in situ formation of Uranus and Neptune via pebble accretion. Astrophys J 931(1):21. https://doi.org/10.3847/1538-4357/ac5f52. arXiv:2203.06545

Von Zahn U, Hunten D (1992) The Jupiter helium interferometer experiment on the Galileo entry probe. Space Sci Rev 60(1–4):263–281. https://doi.org/10.1007/BF00216857

von Zahn U, Hunten DM, Lehmacher G (1998) Helium in Jupiter's atmosphere: results from the Galileo Probe helium interferometer experiment. J Geophys Res 103(E10):22,815–22,830. https://doi.org/10.1029/98JE00695

Vorburger A, Wurz P, Waite H (2020) Chemical and isotopic composition measurements on atmospheric probes exploring Uranus and Neptune. Space Sci Rev 216(4):57. https://doi.org/10.1007/s11214-020-00684-9

Waite JH, Lewis WS, Kasprzak WT, Anicich VG, Block BP, Cravens TE, Fletcher GG, Ip WH, Luhmann JG, Mcnutt RL, Niemann HB, Parejko JK, Richards JE, Thorpe RL, Walter EM, Yelle RV (2004) The Cassini Ion and Neutral Mass Spectrometer (INMS) investigation. Space Sci Rev 114:113–231. https://doi.org/10.1007/s11214-004-1408-2

Waite JH, Burch JL, Brockwell TG, Young DT, Miller GP, Persyn SC, Stone JM, Wilson P, Miller KE, Glein CR, Perryman RS, McGrath MA, Bolton SJ, McKinnon WB, Mousis O, Sephton MA, Shock EL, Choukroun M, Teolis BD, Wyrick DY, Zolotov MY, Ray C, Magoncelli AL, Raffanti RR, Thorpe RL, Bouquet A, Salter TL, Robinson KJ, Urdiales C, Tyler YD, Dirks GJ, Beebe CR, Fugett DA, Alexander JA, Hanley JJ, Moorhead-Rosenberg ZA, Franke KA, Pickens KS, Focia RJ, Magee BA, Hoeper PJ, Aaron DP, Thompson SL, Persson KB, Blase RC, Dunn GF, Killough RL, De Los Santos A, Rickerson RJ, Siegmund OHW (2024) MASPEX-Europa: the Europa Clipper neutral gas mass spectrometer investigation. Space Sci Rev 220(3):30. https://doi.org/10.1007/s11214-024-01061-6

Webster CR, Mahaffy PR (2011) Determining the local abundance of Martian methane and its' 13C/12C and d/h isotopic ratios for comparison with related gas and soil analysis on the 2011 Mars Science Laboratory (msl) mission. Planet Space Sci 59(2):271–283. https://doi.org/10.1016/j.pss.2010.08.021

Webster CR, Mahaffy PR, Flesch GJ, Niles PB, Jones JH, Leshin LA, Atreya SK, Stern JC, Christensen LE, Owen T, Franz H, Pepin RO, Steele A (2013) Isotope ratios of H, C, and O in CO2 and H2O of the Martian atmosphere. Science 341(6143):260–263. https://doi.org/10.1126/science.1237961

Wong MH, Mahaffy PR, Atreya SK, Niemann HB, Owen TC (2004) Updated Galileo Probe Mass Spectrometer measurements of carbon, oxygen, nitrogen, and sulfur on Jupiter. Icarus 171(1):153–170. https://doi.org/10.1016/j.icarus.2004.04.010

Wright IP, Barber SJ, Morgan GH, Morse AD, Sheridan S, Andrews DJ, Maynard J, Yau D, Evans ST, Leese MR, Zarnecki JC, Kent BJ, Waltham NR, Whalley MS, Heys S, Drummond DL, Edeson RL, Sawyer EC, Turner RF, Pillinger CT (2007) Ptolemy—an instrument to measure stable isotopic ratios of key volatiles on a cometary nucleus. Space Sci Rev 128(1–4):363–381. https://doi.org/10.1007/s11214-006-9001-5

Wurz P, Gubler L (1994) Impedance-matching anode for fast timing detectors. Rev Sci Instrum 65:871–876. https://doi.org/10.1063/1.1144914

Wurz P, Gubler L (1996) Fast micro-channelplate detector for particles. Rev Sci Instrum 67:1790–1793. https://doi.org/10.1063/1.1146975

Wurz P, Abplanalp D, Tulej M, Lammer H (2012) A neutral gas mass spectrometer for the investigation of lunar volatiles. Planet Space Sci 74(1):264–269. https://doi.org/10.1016/j.pss.2012.05.016

Wurz P, Rubin M, Altwegg K, Balsiger H, Berthelier JJ, Bieler A, Calmonte U, De Keyser J, Fiethe B, Fuselier SA, Galli A, Gasc S, Gombosi TI, Jäckel A, Le Roy L, Mall UA, Rème H, Tenishev V, Tzou CY (2015) Solar wind sputtering of dust on the surface of 67P/Churyumov-Gerasimenko. Astron Astrophys 583:A22. https://doi.org/10.1051/0004-6361/201525980